

1 **Global and regional emissions estimates of 1,1-difluoroethane (HFC-152a,**
2 **CH₃CHF₂) from in situ and air archive observations.**

3 P. G. Simmonds¹, M. Rigby¹, A.J. Manning², M. F. Lunt¹, S. O'Doherty¹, A. McCulloch¹,
4 P. J. Fraser⁴, S. Henne⁵, M. K. Vollmer⁵, J. Mühle³, R. F. Weiss³, P. K. Salameh³, D. Young¹,
5 S. Reimann⁵, A. Wenger¹, T. Arnold², C.M. Harth³, P. B. Krummel⁴, L. P. Steele⁴, B. L.
6 Dunse⁴, B. R. Miller¹⁴, C. R. Lunder⁶, O. Hermansen⁶, N. Schmidbauer⁶, T. Saito⁷, Y.
7 Yokouchi⁷, S. Park⁸, S. Li⁹, B. Yao¹⁰, L.X. Zhou¹⁰, J. Arduini¹¹, M. Maione¹¹, R.H.J. Wang¹²,
8 D. Ivy¹³ and R. G. Prinn¹³.

9
10 ¹ Atmospheric Chemistry Research Group, University of Bristol, Bristol, BS8 1TS, UK

11 ² Met Office Hadley Centre, Exeter, EX1 3PB, UK

12 ³ Scripps Institution of Oceanography (SIO), University of California San Diego, La Jolla,
13 CA 92093, USA

14 ⁴ CSIRO Oceans and Atmosphere, Aspendale, VIC 3195, Australia

15 ⁵ Laboratory for Air Pollution and Environmental Technology, Swiss Federal Laboratories
16 for Materials Science and Technology (Empa), Dubendorf, CH-8600, Switzerland

17 ⁶ Norwegian Institute for Air Research (NILU), NO-2027 Kjeller, Norway

18 ⁷ Centre for Environmental Measurement and Analysis, National Institute for Environmental
19 Studies, Onogawa, Tsukuba, 305-8506, Japan

20 ⁸ Department of Oceanography, College of Natural Sciences, Kyungpook National
21 University, Daegu, 702-701, Republic of Korea

22 ⁹ Kyungpook Institute of Oceanography, College of Natural Sciences, Kyungpook National
23 University, Daegu, 702-701, Republic of Korea

24 ¹⁰ Chinese Academy of Meteorological Sciences (CAMS), Beijing, 10081, China

25 ¹¹ Department of Basic Sciences and Foundations, University of Urbino, 61029 Urbino, Italy

26 ¹² School of Earth and Atmospheric Sciences, Georgia Institute of Technology, Atlanta,
27 Georgia, USA

28 ¹³ Center for Global Change Science, Massachusetts Institute of Technology, Cambridge, MA
29 02139, USA.

30 ¹⁴ Global Monitoring Division, ESRL, NOAA, Boulder, Colorado, USA

31
32 Correspondence to: P.G. Simmonds (peterssimmonds@aol.com)

33
34 **Abstract**

35 High frequency, in situ observations from eleven globally-distributed sites for the period
36 1994–2014 and archived air measurements dating from 1978 onward have been used to
37 determine the global growth rate of 1,1-difluoroethane (HFC-152a, CH₃CHF₂). These
38 observations have been combined with a range of atmospheric transport models to derive
39 global emission estimates in a top-down approach. HFC-152a is a greenhouse gas with a
40 short atmospheric lifetime of about 1.5 years. Since it does not contain chlorine or bromine,
41 HFC-152a makes no direct contribution to the destruction of stratospheric ozone and is
42 therefore used as a substitute for the ozone depleting chlorofluorocarbons (CFCs) and
43 hydrochlorofluorocarbons (HCFCs). The concentration of HFC-152a has grown substantially
44 since the first direct measurements in 1994, reaching a maximum annual global growth rate
45 of 0.84 ± 0.05 ppt/yr in 2006, implying a substantial increase in emissions up to 2006.
46 However, since 2007, the annual rate of growth has slowed to 0.38 ± 0.04 ppt/yr in 2010 with

47 a further decline to an annual average rate of growth in 2013–2014 of -0.06 ± 0.05 ppt/yr.
48 The annual average Northern Hemisphere (NH) mole fraction in 1994 was 1.2 ppt rising to an
49 annual average mole fraction of 10.1 ppt in 2014. Average annual mole fractions in the
50 Southern Hemisphere (SH) in 1998 and 2014 were 0.84 and 4.5 ppt, respectively. We
51 estimate global emissions of HFC-152a have risen from 7.3 ± 5.6 Gg/yr in 1994 to a
52 maximum of 54.4 ± 17.1 Gg/yr in 2011, declining to 52.5 ± 20.1 Gg/yr in 2014 or 7.2 ± 2.8
53 Tg-CO₂ eq/yr. Analysis of mole fraction enhancements above regional background
54 atmospheric levels suggests substantial emissions from North America, Asia and Europe.
55 Global HFC emissions (so called ‘bottom up’ emissions) reported by the United Nations
56 Framework Convention on Climate Change (UNFCCC) are based on cumulative national
57 emission data reported to the UNFCCC, which in turn are based on national consumption
58 data. There appears to be a significant underestimate (> 20 Gg) of ‘bottom-up’ reported
59 emissions of HFC-152a, possibly arising from largely underestimated USA emissions and
60 undeclared Asian emissions.

61

62 **1. Introduction**

63 HFC-152a (CH₃CHF₂) is primarily sold as an aerosol and foam-blowing agent (Greally
64 et al., 2007) and as a component of some refrigerant blends (Ashford et al., 2004). Emissions
65 to the atmosphere show both temporal and regional variability depending on the specific
66 application in which HFC-152a is used. Incorporation of HFC-152a into aerosol propellants
67 results in prompt release, whereas when used as a single-component non-encapsulated
68 blowing agent, release occurs over a period of about 2 years (McCulloch et al., 2009).
69 Refrigerant use of HFC-152a results in release over longer periods, possibly up to 20 years.
70 Reported emissions of HFC-152a are likely to be incomplete as a consequence of a limited
71 number of producers and confidentiality considerations. Emissions of HFC-152a for some
72 countries are aggregated with other HFCs in a category reported to the UNFCCC as
73 “unspecified mix”. For example, emissions reported by the USA to the UNFCCC for HFC-
74 152a, 227ea, 245ca and 43-10mee are shown in the database as “commercially confidential”
75 and they constitute the aggregated “unspecified” emissions. HFC-152a emissions from the
76 USA are estimated to be the primary contributor to the total for this gas from Annex 1
77 countries (Lunt et al., 2015). Previous papers (Manning and Weiss, 2007; Millet et al., 2009;
78 Stohl et al., 2009; Barletta et al., 2011; Miller et al., 2012; Simmonds et al., 2015) have
79 reported major differences between USA HFC-152a emission estimates derived from
80 atmospheric measurements (top down) and emissions calculated from US reports to the
81 UNFCCC (bottom up). The apparent under-reporting of USA emissions to the UNFCCC
82 ranges from 20–60 Gg based on annual average estimates.

83 HFC-152a has the smallest 100-year global warming potential (GWP_{100} , 138) of all the
84 major HFCs (Forster et al., 2007; Myhre et al., 2013), with a short atmospheric lifetime of 1.5
85 years, due to efficient reaction with tropospheric hydroxyl (OH) radicals (SPARC Report No.
86 6, 2013). Unlike hydrocarbons, HFC-152a does not participate in the reaction to form ozone
87 in the troposphere. These desirable properties have made HFC-152a especially attractive as a
88 replacement, not only for CFCs and HCFCs, but also increasingly for HFC-134a in technical
89 aerosol applications and mobile air-conditioners (IPCC/TEAP, 2011).

90 Ryall et al. (2001) using observations from Mace Head, Ireland reported the
91 distribution of European HFC-152a emissions, concentrated in Germany, and estimated an
92 average European total emission of 0.48 Gg/yr for 1995-1998. Reimann et al. (2004) used a
93 3-year data set (2000–2002) of HFC-152a observations at the Swiss Alpine station
94 Jungfraujoch and trajectory modelling, also noting a predominantly German source for
95 European HFC-152a emissions. This group measured an atmospheric growth rate of 0.3
96 ppt/yr (ppt–parts per trillion, 10^{-12} , mol/ mol or pmol/mol) from 2000 to 2002 and a
97 December 2002 mole fraction at the Jungfraujoch station of 3.2 ppt, from which they
98 estimated a European emission strength of 0.8Gg/yr for 2000–2002.

99 In the Southern hemisphere HFC-152a monthly means, annual means and trends have
100 been reported from observations at Cape Grim, Tasmania, for 1998–2004 (Sturrock et al.,
101 2001; Fraser et al., 2014a; Krummel et al., 2014;). The HFC-152a annual means have grown
102 from 0.8 ppt (0.1 ppt/yr) in 1998 to 1.8 ppt (0.4 ppt/yr) in 2004. More recent estimates of SE
103 Australian HFC-152a emissions (2005–2012) have been calculated by interspecies
104 correlation and model inversions and by extrapolation based on population (Fraser et al.,
105 2014a).

106 Here we further expand the HFC-152a record up to the end of 2014 using in situ
107 observations from eleven globally-distributed monitoring stations (9 Advanced Global
108 Atmospheric Gases Experiment (AGAGE) stations and 2 affiliated stations), together with
109 atmospheric transport models to independently estimate HFC-152a emissions on regional and
110 global scales. We then compare these with HFC-152a emission estimates compiled from
111 national reports to the United Nations Framework Convention on Climate Change
112 (UNFCCC) and Emissions Database for Global Atmospheric Research (EDGAR v4.2;
113 <http://edgar.jrc.ec.europa.eu/>), using the same techniques reported for other greenhouse gases
114 (O’Doherty et al., 2009, 2014; Miller et al., 2010; Vollmer et al., 2011; Krummel et al., 2014;
115 Rigby et al., 2014).

116

117 2. Experimental methods

118 2.1 Instrumentation and Calibration

119
120 High frequency, in situ measurements of HFC-152a were made by gas
121 chromatography-mass spectrometry (GC-Agilent 6890) coupled with quadrupole mass
122 selective detection (MSD-Agilent 5973/5975). Measurements commenced at Mace Head,
123 Ireland in 1994 and Cape Grim, Tasmania in 1998, using a custom-built automated pre-
124 concentration system (Adsorption Desorption System -ADS) to selectively and quantitatively
125 retain halogenated compounds from 2 L air samples. Based on a Peltier-cooled pre-
126 concentration microtrap cooled to -50°C during the adsorption phase, the ADS provided on
127 site calibrated air samples every 4 hours, i.e. 6 per day (Simmonds et al., 1995). In 2004 the
128 ADS-GC-MS was replaced with a more advanced custom-built pre-concentration system
129 (Medusa) with enhanced cooling to $\sim -180^{\circ}\text{C}$ and the relatively mild adsorbent HayeSep D
130 (Miller et al., 2008; Arnold et al., 2012). Agilent 5973 MSDs (mass selective detector) were
131 also upgraded to the Agilent 5975 MSDs over the course of the Medusa observations.
132 Analysis of each 2 L sample of ambient air was alternated with analysis of a 2 L reference
133 gas (designated as a working standard) to correct for short-term instrumental drift, resulting
134 in 12 (Medusa) individually calibrated air measurements per day. Working standards were
135 prepared for each station by compressing ambient air into 34 L electropolished stainless steel
136 canisters (Essex Industries, Inc., Missouri) using modified oil-free compressors (SA-6, RIX,
137 California). Exceptions to this were the Cape Grim and Zeppelin stations, where the working
138 standards were filled using a cryogenic filling technique. Research-grade helium, which was
139 used as a carrier gas in the Medusa systems, was further purified by passage through a heated
140 “getter” type purifier (Valco Instruments, Houston, TX). The carrier gas was analysed for
141 blanks on a regular basis and blank levels of HFC-152a were below the limit of detection at
142 all field stations.

143 Table 1 lists the geographical location and the time when routine ambient
144 measurements of HFC-152a began at each monitoring station. Stations with the longest
145 observational records that deployed both ADS and Medusa GC-MS instruments include
146 Mace Head (MHD), Jungfrauoch (JFJ), Ny-Ålesund (ZEP) and Cape Grim (CGO). Medusa
147 GC-MS instruments were installed at five other AGAGE stations Trinidad Head (THD),
148 Gosan (GSN), Ragged Point, (RPB), Shangdianzi (SDZ) and Cape Matatula (SMO) between
149 2003 and 2010. In addition two AGAGE affiliated stations Monte Cimone (CMN) and
150 Hateruma (HAT), which use comparable GC-MS instruments, but a different pre-

151 concentration design for sample enrichment, commenced HFC-152a measurements in 2001
152 and 2004, respectively. Importantly, all eleven stations listed in Table 1 report HFC-152a
153 measurements relative to the Scripps Institution of Oceanography (SIO-05) calibration scale
154 (as dry gas mole fractions in pmol/mol).

155
156 The estimated accuracy of the calibration scale for HFC-152a is 4%: a more detailed
157 discussion of the measurement technique and calibration procedure is reported elsewhere
158 (Miller et al., 2008; O'Doherty et al., 2009; Mühle et al., 2010). HFC-152a was determined
159 using the MS in selected ion monitoring mode (SIM) with a target ion CH_3CF_2^+ (m/z 65) and
160 qualifier ion CH_3CF^+ (m/z 46). To ensure that potential interferences from co-eluting species
161 did not compromise the analysis, the ratio of the target to qualifier ion was continuously
162 monitored. Measurement precision was calculated as the daily standard deviation (1σ) of the
163 ratios of each standard response to the average of the closest-in-time preceding and
164 subsequent standard responses. Typical daily precisions vary from station to station with a
165 range of 0.1–0.4 ppt. Individual station precisions were used to estimate the precision of each
166 in situ measurement.

167 168 *2.2 Northern and Southern Hemisphere archived air samples*

169
170 In order to extend the HFC-152a data record back before the commencement of high-
171 frequency measurements, analyses of Northern Hemisphere (NH) and Southern Hemisphere
172 (SH) archived air samples dating back to 1978, were carried out using three similar Medusa
173 GC-MS instruments at the Scripps Institution of Oceanography (SIO), La Jolla, California,
174 the Commonwealth Scientific and Industrial Research Organisation (CSIRO), Aspendale,
175 Australia and the Cape Grim Baseline Station, Tasmania. The SH samples are part of the
176 Cape Grim Air Archive (CGAA) described in Langenfelds et al., (1996); and Krummel et al.,
177 (2007). The NH samples analysed for this paper were filled during background conditions
178 mostly at Trinidad Head, but also at La Jolla, California; Cape Meares, Oregon; Ny Ålesund,
179 Svalbad and Point Barrow, Alaska (some samples are courtesy of the National Oceanic and
180 Atmospheric Administration (NOAA)).

181 In addition, eight SH samples were measured at SIO and compared with SH samples
182 of similar age measured at CSIRO (February 1995, July 1995, November 1995, June 1998,
183 July 2004, February 2006, August 2008, and December 2010, $\Delta x = 0.01$ – 0.07 ppt $\Delta t = 1$ – 33
184 days) and three NH samples were measured at CSIRO and compared with NH samples of the
185 same age measured at SIO (May 1989 and April 1999, $\Delta x = 0.02$ – 0.06 ppt, $\Delta t = 1$ – 11 days).

186 The good agreement between SIO and CSIRO archived air stored in different types of tanks
187 (stainless steel tanks, Essex Industries, Inc and Silcosteel treated tanks, Restek Corporation)
188 serves both as proof of the good consistency of the individual Medusa GC-MS instruments
189 and the integrity of the tanks used. Samples were analysed in replicate typically 3–6 times
190 each and several NH tanks were re-measured over a number of years.

191 192 *2.3 Selection of baseline data*

193
194 Baseline in situ monthly mean HFC-152a mole fractions were calculated by excluding
195 values enhanced by local and regional pollution influences, as identified by the iterative
196 AGAGE pollution identification algorithm, (see Appendix in O’Doherty et al., 2001).
197 Briefly, baseline measurements are assumed to have a Gaussian distribution around the local
198 baseline value, and an iterative process is used to filter out the points that do not conform to
199 this distribution. A second-order polynomial is fitted to the subset of daily minima in any
200 121-day period to provide a first estimate of the baseline and seasonal cycle. After
201 subtracting this polynomial from all the observations a standard deviation and median are
202 calculated for the residual values over the 121-day period. Values exceeding three standard
203 deviations above the baseline are thus identified as non-baseline (polluted) and removed from
204 further consideration. The process is repeated iteratively to identify and remove additional
205 non-baseline values until the new and previous calculated median values agree within 0.1%.
206 For the core AGAGE stations, in situ baseline data and archive air data, extending the record
207 to periods prior to the in situ measurement period, are then combined for each hemisphere,
208 and outliers are rejected by a similar iterative filtering process.

209

210 **3. Modelling studies**

211

212 We pursued several approaches to determine emissions at global, continental and
213 regional scales. The methodologies have been published elsewhere and are summarised
214 below. The global, continental and some regional estimates incorporate a priori estimates of
215 emissions, which were subsequently adjusted using the observations.

216 There are several sources of information on production and emissions of HFC-152a; none of
217 which, on their own, provides a complete database of global emissions. The more
218 geographically comprehensive source of information is provided by the parties to the
219 UNFCCC, but only includes Annex 1 countries (developed countries). The 2014 database
220 covers years 1990 to 2012 and are reported in Table 2(II) s1 in the Common Reporting

221 Format (CRF) available at [http://unfccc.int/national](http://unfccc.int/national_reports/annex_ghg_inventories/national)
222 [reports/annex_ghg_inventories/national](http://unfccc.int/national_reports/annex_ghg_inventories/national_reports_submissions/items/8108.php)
223 [inventories_submissions/items/8108.php](http://unfccc.int/national_reports/annex_ghg_inventories/national_reports_submissions/items/8108.php). An alternative inventory estimate was also obtained
224 from the Emissions Database for Global Atmospheric Research (EDGAR v4.2;
225 <http://edgar.jrc.ec.europa.eu/>), a database that estimates global emission inventories of
226 anthropogenic greenhouse gases (GHGs) on a country, region and grid basis up to 2008.

227 To infer “top-down” emissions we select observations from the various observing sites
228 listed in Table 1 and four chemical transport models. These eleven sites are sensitive to many
229 areas of the world in which HFC-152a emissions are reported, however other areas of the
230 globe that are not well monitored by this network are also likely to have significant emissions
(such as South Asia, South Africa, and South America).

231 232 *3.1 Global emissions estimates using the AGAGE two-dimensional 12-box model* 233

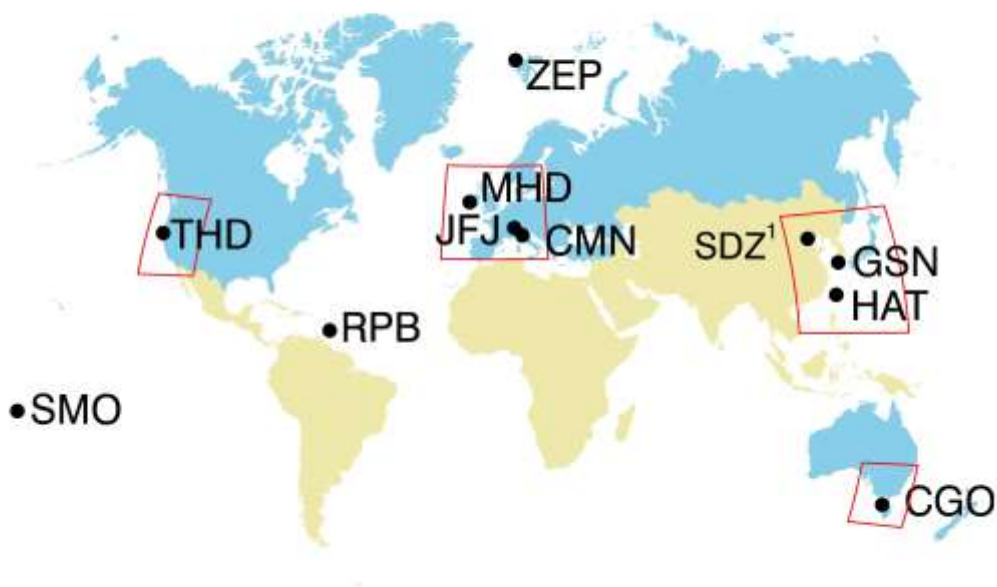
234 To estimate global-average mole fractions and derive growth rates, a two-dimensional
235 model of atmospheric chemistry and transport was employed. The AGAGE 12-box model
236 simulates trace gas transport in four equal mass latitudinal sections (divisions at 30-90°N, 0-
237 30°N, 30-0°S and 90-30°S) and at three heights (vertical divisions at 200, 500 and 1000 hPa).
238 The model was originally developed by Cunnold et al. (1983) (nine-box version), with
239 subsequent improvements by Cunnold et al. (1994) and Rigby et al. (2013, 2014). Emissions
240 were estimated between 1989 and 2014 using a Bayesian method in which an a priori
241 constraint (EDGAR v4.2) on the emissions growth rate was adjusted using the baseline-
242 filtered AGAGE observations (Rigby et al., 2011a, 2014). Global emissions were derived that
243 included estimates of the uncertainties due to the observations, the prior and the lifetime of
244 HFC-152a, as detailed in the supplementary material in Rigby et al. (2014). Note that
245 historically and here the 12-box model only uses observations from the core AGAGE sites,
246 Mace Head, Trinidad Head, Ragged Point, Cape Matatula, and Cape Grim.

247 248 *3.2 Global and continental emissions estimates using a combined Eulerian and Lagrangian* 249 *model* 250

251 We used the methodology outlined in Lunt et al. (2015) and Rigby et al. (2011b) to
252 derive emissions of HFC-152a from continental regions. The high-resolution, regional UK
253 Met Office Numerical Atmospheric dispersion Modelling Environment (NAME), Manning et
254 al. (2011) was used to simulate atmospheric HFC transport close to a subset of AGAGE
255 monitoring sites, which were strongly influenced by regional HFC sources (domains shown
256 by red boxes in Figure 1). Simultaneously, the influence of changes to the global emissions

257 field on all measurement stations was simulated using the global Model for Ozone and
 258 Related Tracers, MOZART (Emmons et al., 2010). We estimated annual emissions for the
 259 period 2007-2012 and aggregated the derived emissions fields into continental regions,
 260 separating countries that either do (“Annex-1”), or do not (“non-Annex-1”) report detailed,
 261 annual emissions to the UNFCCC. Emissions were estimated using a hierarchical Bayesian
 262 inverse method (Ganesan et al., 2014, Lunt et al., 2015) and all high-frequency observations
 263 from 10 of the 11 sites listed in Table 1, excluding Shangdianzi due to the short time series.
 264 The hierarchical Bayesian method includes uncertainty parameters (e.g. model “mismatch”
 265 errors and a priori uncertainties) in the estimation scheme, reducing the influence of
 266 subjective choices on the outcome of the inversion.

267



291

292 Figure 1. Location of AGAGE and affiliated stations.
 293 Ny-Ålesund, Zeppelin, Norway (ZEP); Mace Head, Ireland (MHD); Jungfrauoch,
 294 Switzerland (JFJ); Monte Cimone, Italy (CMN);Trinidad Head, USA (THD); Shangdianzi,
 295 China (SDZ); Gosan, South Korea (GSN); Hateruma, Japan (HAT); Ragged Point, Barbados
 296 (RPB); Cape Matatula, American Samoa (SMO); and Cape Grim, Tasmania (GCO). Red
 297 boxes indicate “local regions” where the NAME model was used with increased resolution
 298 compared to the global MOZART model, Annex 1 countries are shaded blue and non-Annex
 299 1 countries are shaded yellow.
 300 Note: ¹ Shangdianzi (SDZ) was not used in any of the modelling studies due to the relatively
 301 short time series.

302 *3.3 High-resolution regional emissions estimates using InTEM*

303

304 A method for estimating emissions from observations and atmospheric transport
305 modelling with NAME referred to as InTEM, ‘Inversion Technique for Emission Modelling’
306 (Manning et al., 2011), uses a simulated annealing method (Press et al., 1992) to search for
307 the emission distribution that produces a modelled times-series that has the best statistical
308 match to the observations from certain AGAGE stations (e.g. Mace Head, Cape Grim).
309 NAME was driven with output from the operational analysis of the UK Met Office
310 Numerical Weather Prediction model, the Unified Model, at global horizontal resolution of
311 17-40 km (year dependent). InTEM estimates the spatial distribution of emissions across a
312 defined geographical area, and can either start from a random emission distribution or be
313 constrained by an inventory-defined distribution. Emission totals from specific geographical
314 areas are calculated by summing the derived emissions from each grid (non-uniform) in that
315 region.

316 The uncertainty estimation used within InTEM is described in detail elsewhere
317 (Manning et al 2011). Briefly, the uncertainty space was explored by a) solving the inversion
318 multiple times with a range of baseline mole fractions within the baseline uncertainty
319 estimated during the baseline fitting process and b) by altering the 3-year inversion time
320 window by one month throughout the data period thereby solving over a particular one year
321 period many times using different observations. In total for each annual estimate up to 111
322 inversions were performed, the median and 5th and 95th percentiles were used as the final total
323 and spread. For the Australian estimates data between 2002 through 2011 were used, for the
324 NW European estimates data between Nov. 1994 and Dec. 2013 were used.

325 *3.4 High resolution European emission estimates using the FLEXPART model*

326 A regional Bayesian inversion system using backward simulations of a Lagrangian
327 particle dispersion model FLEXPART (Stohl et al., 2005) was applied to the HFC-152a
328 observations from Mace Head, Jungfraujoch and Mt. Cimone for the period 2006 to 2014.
329 The inversion technique follows the description by Stohl et al. (2009) and was previously
330 applied to regional halocarbon emissions from Europe (Keller et al., 2012, Maione et al.,
331 2014) and China (Vollmer et al., 2009). For these emission estimates, the background was
332 determined by applying the Robust Extraction of Baseline Signal (REBS) filter described in
333 detail by (Ruckstuhl et al., 2012). The transport model FLEXPART was driven with output
334 from the operational analysis of the Integrated Forecast System (IFS) of the European Centre

335 for Medium Range Weather Forecast (ECMWF) using a spatial resolution of $0.2^\circ \times 0.2^\circ$ for a
336 nested domain covering the larger area of the European Alps and a spatial resolution of $1^\circ \times$
337 1° elsewhere.

338 The FLEXPART model was applied to the HFC-152a observations from Mace Head,
339 Jungfraujoch and Mt. Cimone for the period 2006 to 2014. Prior to 2006, the model
340 resolution of Integrated Forecast System (IFS) was not sufficiently fine to realistically
341 simulate the transport to the two high altitude sites Jungfraujoch and Mt. Cimone. Therefore,
342 no attempt was made here to apply the inversion system to years before 2006. As prior
343 information of the HFC-152a emissions we used country totals as submitted to UNFCCC.
344 These were spatially disaggregated following the HFC-152a distribution given in EDGAR
345 (v4.2). For countries not reporting HFC-152a emissions to UNFCCC we used the values
346 given in EDGAR. The EDGAR inventory was only available up to the year 2008 beyond this
347 year the EDGAR 2008 distribution was used. The uncertainty of the prior emissions was set
348 so that the region total uncertainty equalled 20 % of the region total emissions. The regional
349 inversion grid covered a region similar to that shown in Figure 1.

350

351 *3.5 Regional emissions estimates using the inter-species correlation (ISC) methods*

352 We also present regional emissions estimates using inter-species correlation (ISC)
353 methods (Yokouchi et al., 2005). Emissions of a number of trace gases from the
354 Melbourne/Port Phillip region (CFCs, HCFCs, HFCs, carbon tetrachloride: Dunse et al.,
355 2001, 2002, 2005; O'Doherty et al., 2009; Fraser et al., 2014a, b), including HFC-152a
356 (Greally et al., 2007), have been estimated utilising in situ high frequency measurements
357 from Cape Grim and ISC with co-incident carbon monoxide (CO) measurements.

358 ISC works best for co-located sources – however extensive modelling has shown that
359 by the time the Melbourne/Port Phillip plume reaches Cape Grim (300 km from the source) it
360 is well mixed and the likely inhomogeneity of the source regions (for CO and HFC-152a in
361 this case) does not have a significant influence on the derived emissions. It should be noted
362 that in order to obtain a significant sampling of Port Phillip pollution episodes at Cape Grim,
363 data from 3 years (for example 2011-2013) are used to derive annual emissions (for 2012).
364 (InTEM also uses data from 3 years to derive annual emissions.) The ISC uncertainties given
365 in the paper include (1) the uncertainties in the estimates of CO emissions from
366 Melbourne/Port Phillip (2) the uncertainties in the overall correlation between CO and

367 HCFC-152a as seen in pollution episodes at Cape Grim (3) the uncertainties in the
368 geographic extent of the HFC-152a and CO source regions impacting on Cape Grim and their
369 entrained population.

370 Using HCFC-22 as the reference tracer, Li et al., (2011) reported that China is the
371 dominant emitter of halocarbons in East Asia. North American HFC-152a emissions have
372 been estimated from atmospheric data using interspecies correlation based techniques with
373 CO (Millet et al., 2009, Barletta et al., 2011) and fossil fuel CO₂ (Miller et al., 2012) as the
374 reference emissions.

375 **4. Results and Discussion**

376

377 *4.1 In situ observations*

378

379 The time series of HFC-152a in situ observations recorded at selected AGAGE and
380 affiliated monitoring stations are shown in Figure 2 (a-c). Data have been filtered into
381 baseline (black) and above baseline (red) using the AGAGE pollution algorithm, as discussed
382 in section 2.3. Figure 2a shows the mole fractions in ppt for the four stations that deployed
383 both ADS and Medusa GC-MS instruments (Mace Head, Zeppelin, Jungfraujoch, and Cape
384 Grim). Most notable are the substantial above baseline events at Mace Head and Jungfraujoch
385 that are influenced primarily by emissions from European sources. Conversely, the Zeppelin
386 Arctic station and the SH station at Cape Grim have relatively small above baseline events
387 implying smaller emissions from local or regional sources.

388

389

390

391

392

393

394

395

396

397

398

399

400

401
402
403
404
405
406
407
408
409
410
411
412
413
414
415
416
417
418
419
420
421
422
423
424
425
426
427
428
429
430
431
432
433
434
435
436
437
438
439
440
441
442

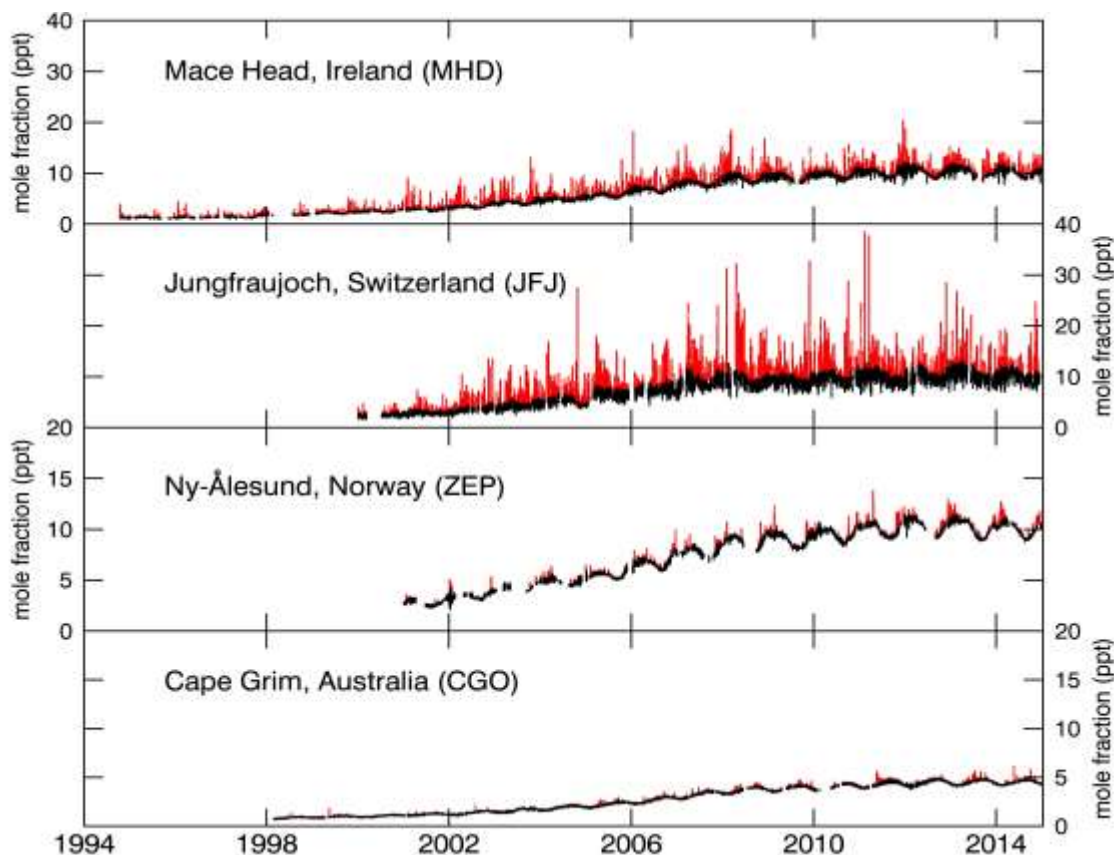
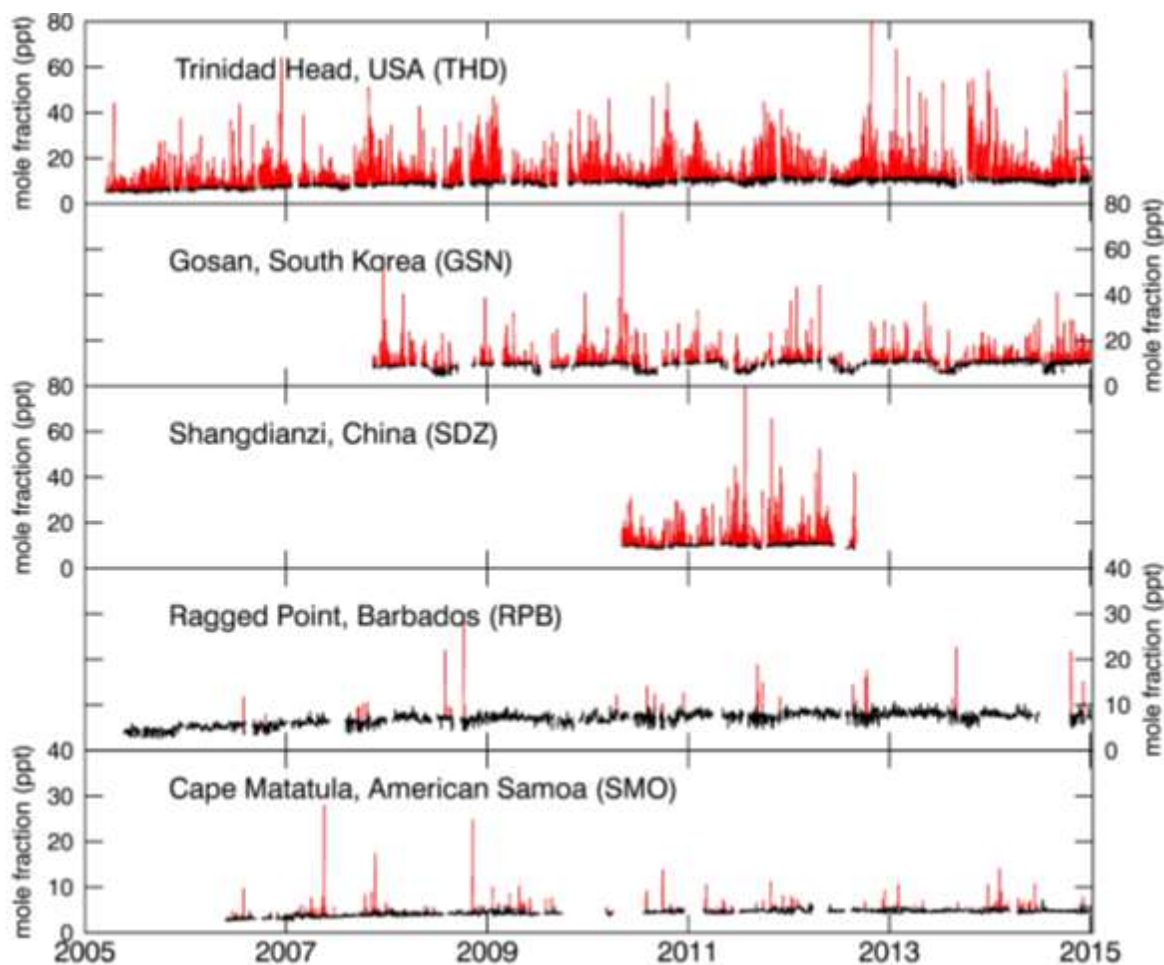


Figure 2a. Time series of HFC-152a mole fractions (ppt) recorded at the four monitoring stations with combined ADS and Medusa data. (MHD, JFJ, ZEP and CGO), (note the different Y-axis scales). Data have been assigned as baseline (black) and non-baseline (red) using the AGAGE pollution identification algorithm.

Figure 2b shows measurements at the five other AGAGE stations (Trinidad Head, Gosan, Ragged Point, Shangdianzi, and Cape Matatula), which used only Medusa GC-MS instruments. The North American site at Trinidad Head and the Asian sites at Shangdianzi and Gosan are the most strongly influenced by regional emissions. The tropical sites at Ragged Point, Barbados and Cape Matatula, American Samoa show very few enhancements above the baseline and these are due mostly to local emissions occurring under night time inversion conditions and occasional influences from regional emission sources (note the different Y-axis scales). Although the Shangdianzi station was operational for only a short period, the enhancements above baseline are significant due to the sensitivity of this site to Chinese emissions, and comparable in magnitude to those at Gosan.

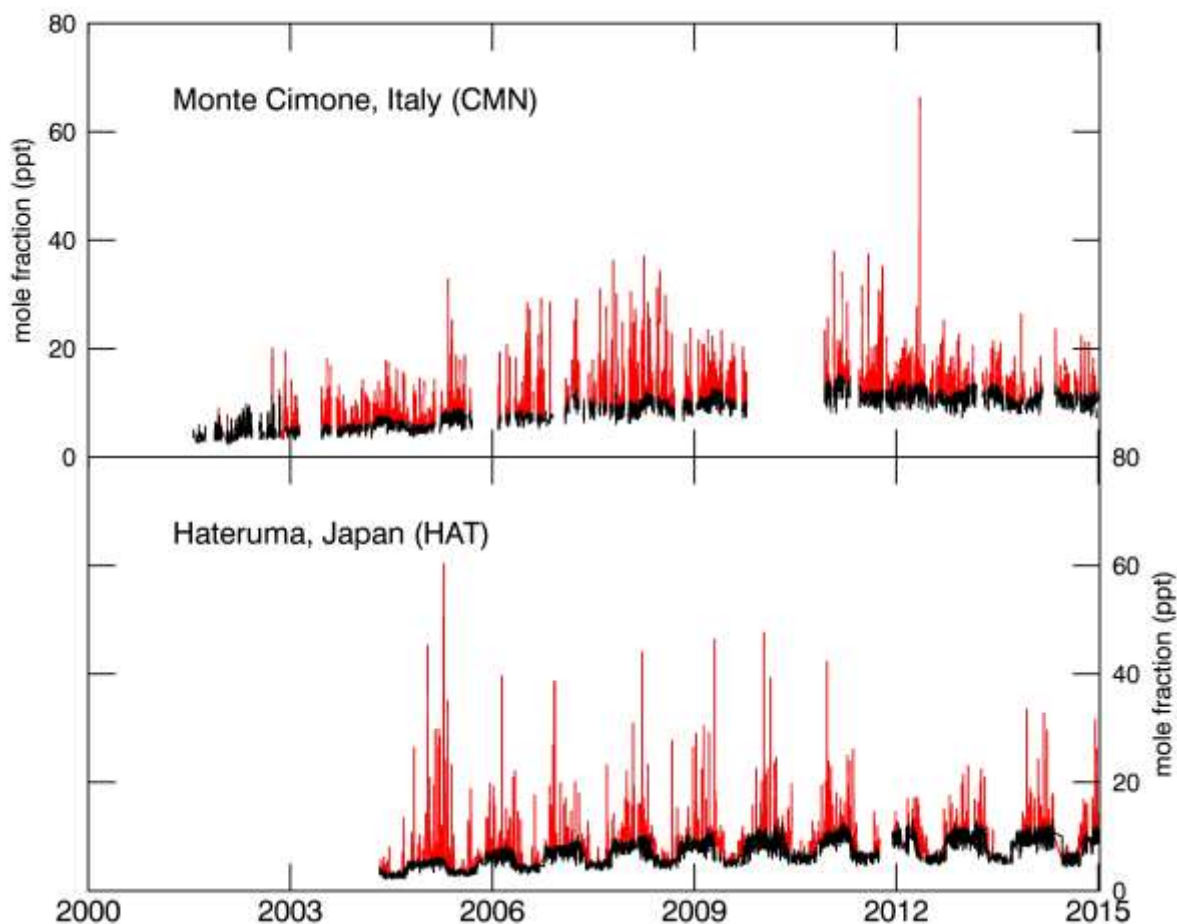


443
444
445
446
447
448
449
450

Figure 2b. Time series of HFC-152a mole fractions (ppt), recorded with the Medusa GC-MS instruments at the five AGAGE monitoring stations (THD, GSN, SDZ, RPB, and SMO). Data have been assigned as baseline (black) and non-baseline (red) using the AGAGE pollution identification algorithm.

451 Figure 2c illustrates the time series from the two affiliated AGAGE stations (Monte
452 Cimone and Haturuma) that used comparable GC-MS instruments but with different methods
453 of pre-concentration. Monte Cimone, like the Jungfrauoch, is also influenced by substantial
454 emissions from sources in continental Europe. Haturuma is influenced by sources in China,
455 Korea, Taiwan and Japan (Yokouchi et al., 2006).

456
457
458
459
460
461
462
463
464

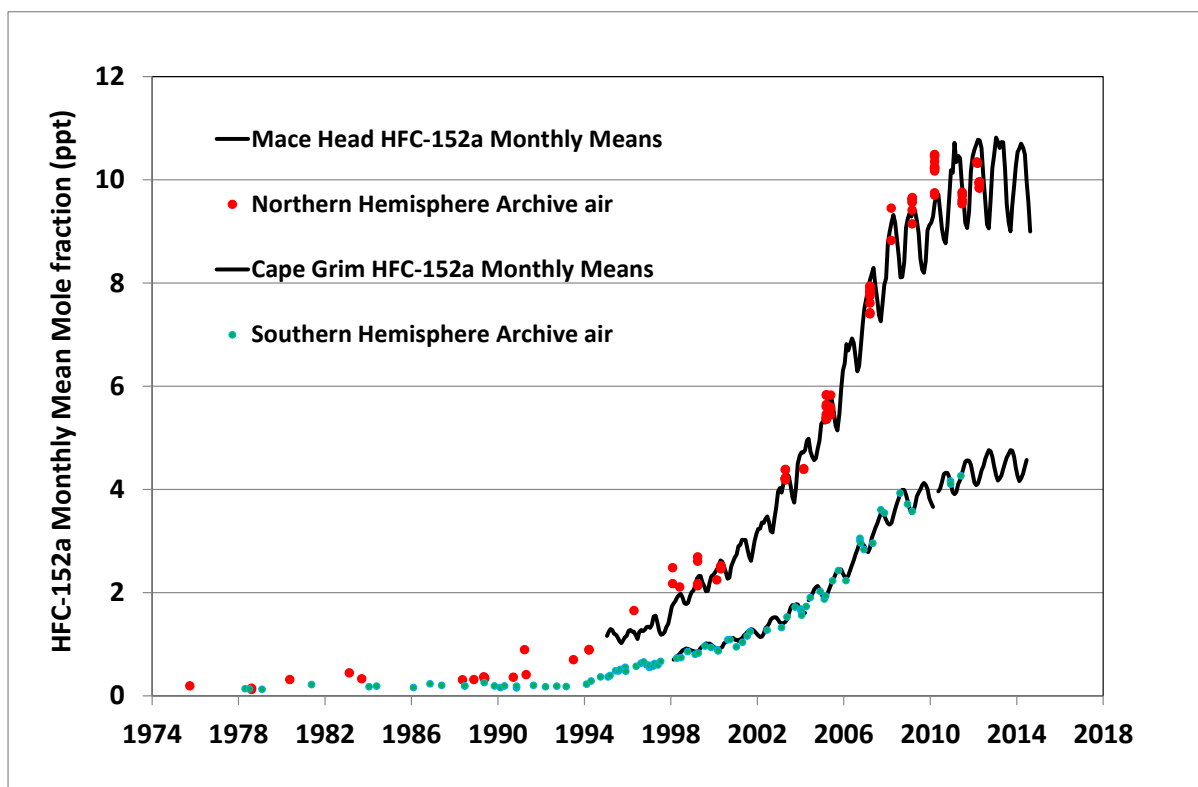


465
 466 Figure 2c. Time series of HFC-152a mole fractions (ppt) recorded with the GC-MS
 467 instruments at the two affiliated AGAGE stations CMN and HAT. Data have been assigned
 468 as baseline (black) and non-baseline (red) using the AGAGE pollution identification
 469 algorithm.

470
 471 *4.2 Atmospheric Trends and Seasonal Cycles*

472
 473 Figure 3 shows the in situ measurements of HFC-152a, as baseline monthly means
 474 (excluding pollution events), obtained from the two AGAGE stations Mace Head and Cape
 475 Grim with the longest time series that deployed both ADS and Medusa GC-MS instruments.
 476 Superimposed in Figure 3 are the NH and SH archived flask data extending back to 1978.
 477 Annual average mole fractions at Mace Head increased from 1.2 ppt in 1994 to 10.2 ppt by
 478 2014, Cape Grim annual average mole fractions increased from 0.84 ppt in 1998 when in situ
 479 measurements first began to 4.5 ppt in 2014. However, in the last few years the rates of
 480 growth at both sites have slowed to almost zero.

481
 482
 483
 484

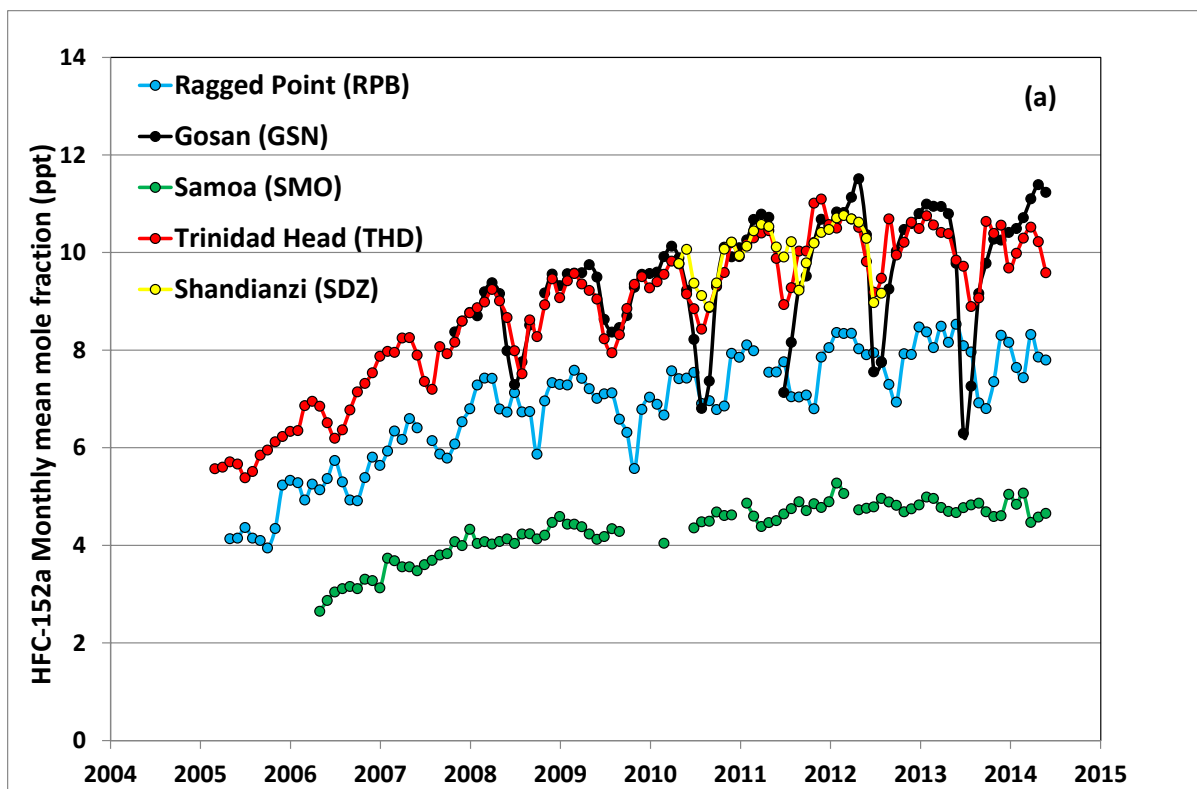


485
 486 Figure 3. HFC-152a baseline monthly mean mole fraction (ppt) recorded at Mace Head-
 487 MHD (ADS GC-MS, 1994-2003; Medusa GC-MS, 2004-2014) and at Cape Grim-CGO
 488 (ADS GC-MS, 1998-2003; Medusa GC-MS, 2004-2014) and from analysis of archived NH
 489 and SH air samples extending back to 1975: in situ (black), air archive NH (red) and SH
 490 (blue).

491
 492 The NH archived samples are more variable than the SH archived samples. The SH archive is
 493 collected only under strict baseline conditions (Southern Ocean air) and is far removed from
 494 the major sources of HFC-152a. Conversely in the NH, where most major sources of
 495 emissions are located, sampling under strict baseline conditions is more difficult to achieve.

496
 497 Figure 4a illustrates HFC-152a baseline monthly means obtained from the five other
 498 AGAGE observing sites (Ragged Point, Gosan, Cape Matatula, Trinidad Head and
 499 Shangdianzi using only the more advanced Medusa GC-MS. There is a large seasonal cycle
 500 at Gosan with a very deep minimum due to summertime transport from the Southern
 501 Hemisphere (Li et al., 2011). Barbados can also be influenced by southern hemispheric air
 502 during the hurricane season (Archibald et al., 2015).

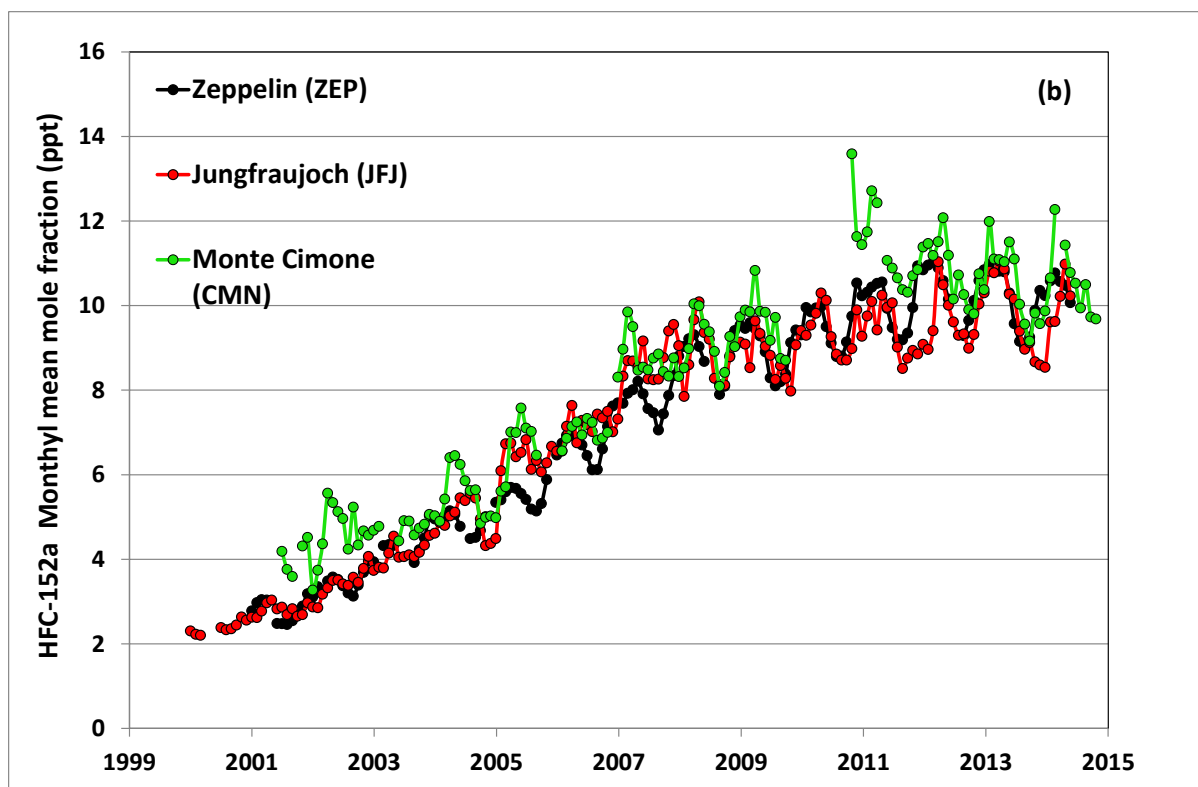
503
 504
 505
 506



507
 508 Figure 4a. Medusa GC-MS baseline monthly mean mole fractions (ppt) recorded at Ragged
 509 Point, Gosan, Cape Matatula, Trinidad Head, and Shangdianzi. Observations at Shangdianzi
 510 were discontinued in August 2012.

511
 512 Figure 4b shows the baseline monthly mean mole fractions for the three mountain
 513 stations. Ny-Ålesund and Jungfraujoch, using combined ADS and Medusa GC-MS
 514 measurements and Monte Cimone, which used a commercial pre-concentrator GC-MS. In
 515 most years Monte Cimone exhibits enhanced mole fractions during the NH spring months
 516 (March–May).

517
 518
 519
 520
 521
 522
 523
 524
 525
 526
 527
 528
 529
 530



531

532 Figure 4b. Combined ADS and Medusa GC-MS baseline monthly mean mole fraction
 533 recorded at Ny-Ålesund, Jungfrauoch and Monte Cimone.

534

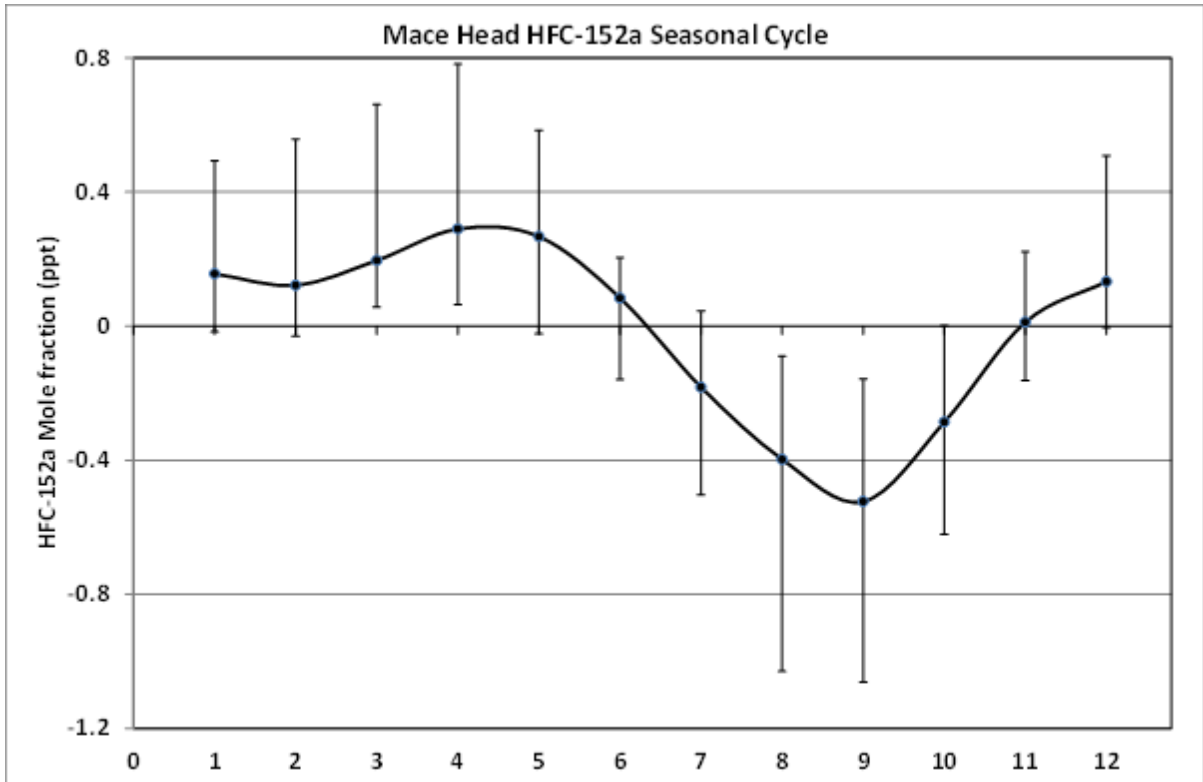
535 The HFC-152a seasonal cycles at Mace Head and Cape Grim shown in Figures 5a and
 536 5b, are broadly representative of the Northern and Southern Hemispheres, respectively. The
 537 seasonal cycle at Mace Head shows a NH spring maximum (April-May) and late summer
 538 minimum (August-October), while the SH seasonal cycle at Cape Grim exhibits a broad
 539 austral spring maximum (July-November) and a late summer minimum (January-April). The
 540 summer minimum at both locations is attributed to enhanced summertime loss (OH) with
 541 possibly a contribution from seasonally varying emissions in the NH that may be out-of-
 542 phase with the NH sink. At Cape Grim an additional source of seasonality is due to
 543 seasonally varying transport between the NH and SH, which is generally in phase with the
 544 sink induced seasonal cycle. This competition between OH summertime loss and seasonally
 545 varying transport has been observed at many other AGAGE locations (Prinn et al., 1992;
 546 Greally et al., 2007; O'Doherty et al., 2009, 2014 and Li et al., 2011).

547

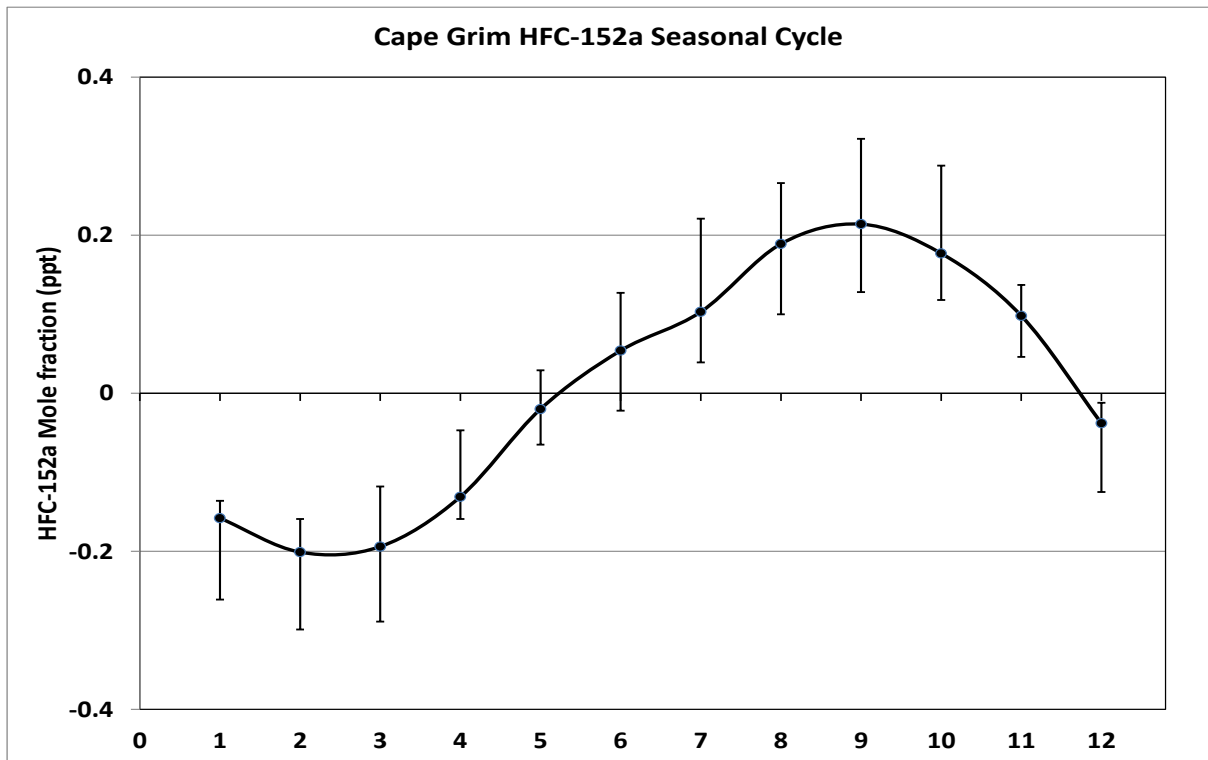
548

549

550

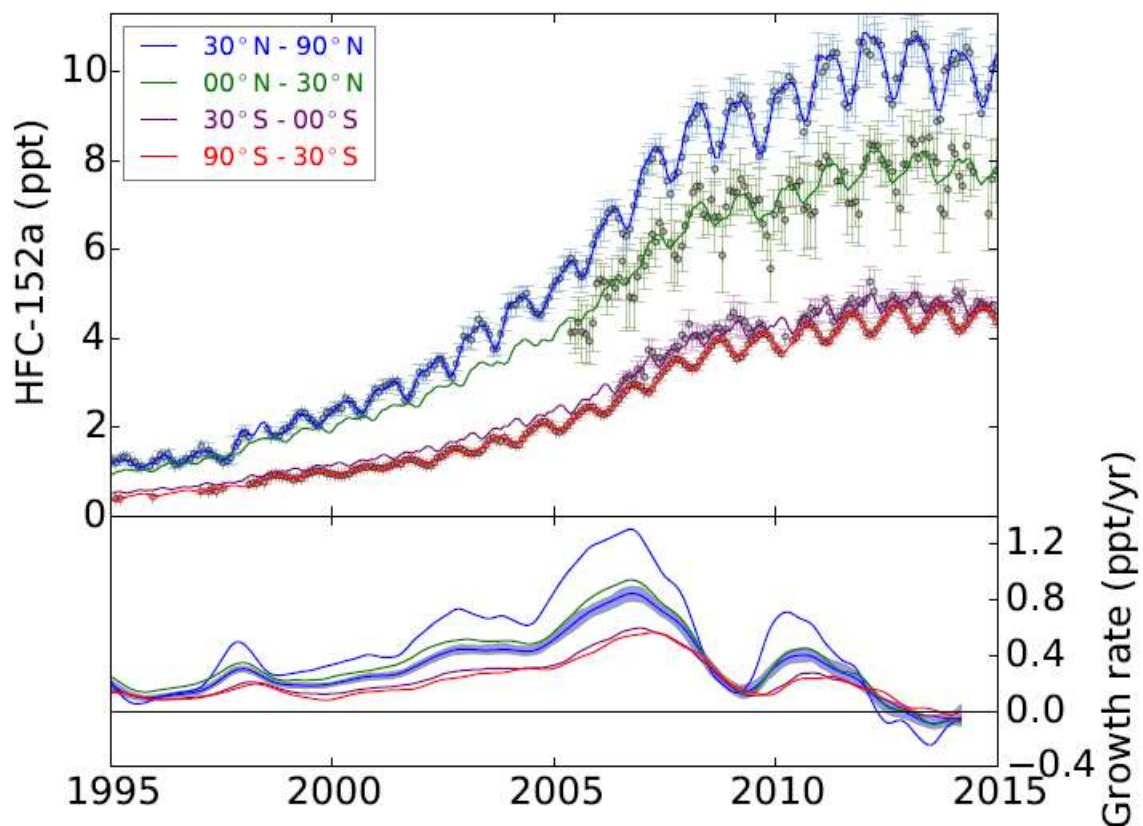


551
 552 Figure 5a. Average seasonal cycle at Mace Head, Ireland (2004-2014). Black line represents
 553 the average for each month of these individual years and the error bars represent the min to
 554 max range.



555
 556 Figure 5b. Average seasonal cycle at Cape Grim, Tasmania (2004-2014). Black line
 557 represents the average for each month of these individual years and the error bars represent
 558 the min to max range.

559 Figure 6 shows the mole fractions output from the AGAGE global 12-box model,
 560 along with the monthly-mean semi-hemispheric average observations used in the inversion.
 561 The figure also shows the running mean growth rate, smoothed using a Kolmogorov–
 562 Zurbenko filter with a window of approximately 12 months (Rigby et al., 2014). Most
 563 notable is the positive growth rate from 1995 reaching a maximum of ~ 0.84 ppt/yr in 2006,
 564 followed by a steady decline in the growth rate with a minimum in 2008-2009 during the time
 565 of the economic recession. The positive growth rate then resumes increasing to ~ 0.4 ppt/yr in
 566 2010 followed by a subsequent decrease with an annual average growth rate in 2013-2014 of
 567 minus ~ 0.06 ppt/yr.



568 Figure 6. Top panel: AGAGE 12-box model mole fractions (solid line) for the two
 569 NH ($30^{\circ}\text{N}-90^{\circ}\text{N}$, MHD and THD and $00^{\circ}\text{N}-30^{\circ}\text{N}$, RGP) and the two SH ($30^{\circ}\text{S}-00^{\circ}\text{S}$,
 571 SMO and $90^{\circ}\text{S}-30^{\circ}\text{S}$, CGO) latitudinal bands. The points show the semi-hemispheric
 572 monthly mean observations from the 5 AGAGE stations used in the inversion (MHD,
 573 THD, RPB, SMO, CGO). Lower panel: HFC-152a annualized growth rate (see Rigby
 574 et al., 2014 for smoothing method) for each semi-hemisphere, with the heavy blue line
 575 and shading showing the global average and its uncertainty.
 576
 577

578 The strong inter-hemispheric gradient demonstrates that emissions are predominantly
579 in the NH, as has been illustrated for many other purely anthropogenic trace gases (Prinn et
580 al., 2000). The globally averaged mole fraction in the lower troposphere in 2014 is estimated
581 to be 6.84 ± 0.23 ppt and the annual rate of increase is -0.06 ± 0.05 ppt/yr. As reported by
582 Rigby et al. (2014) the major long lived synthetic greenhouse gases (SGHG) which include
583 CFCs, HCFCs, HFCs and perfluorocarbons (SF_6 and NF_3), as well as CH_3CCl_3 and CCl_4
584 were responsible for 350 ± 10 mW/m² of direct radiative forcing in 2012. The radiative
585 forcing of HFC-152a, determined from the AGAGE 12-box model in this study, was $0.61 \pm$
586 0.02 mW/m² in 2014, which represents only a tiny fraction (~0.2%) of the global radiative
587 forcing of the SGHG.

588

589 **5. Top-down Emission Estimates**

590

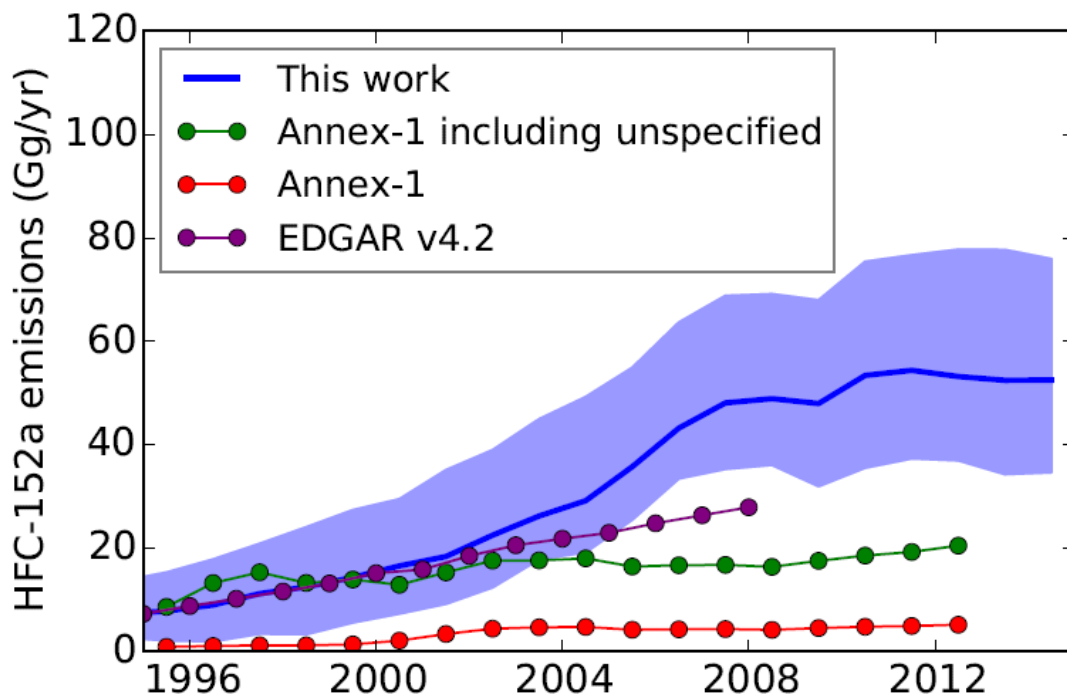
591 *5.1 Global estimates*

592

593 Estimated global emissions of HFC-152a using the 12-box model and the reported
594 UNFCCC and EDGAR emission inventories are shown in Figure 7 and Table 2. The blue
595 solid line represents our model-derived emissions, with the 1σ error band shown by the
596 shaded areas. Model derived emissions grew steadily from 1995-2007 with a non-
597 statistically-significant decrease in emissions in 2009 to 48 ± 16.4 Gg/yr, during the time of
598 the economic downturn in 2008-2009. The mean emission reached a maximum of 54.4 ± 17.1
599 Gg/yr in 2011, followed by a period of relatively stable emissions, the mean showing a slight
600 decline to 52.5 ± 20.1 Gg/yr (7.2 ± 2.8 Tg-CO₂ eq/yr) in 2014.

601

602



603 Figure 7. HFC-152a emissions estimates derived from observations (blue line and shading,
 604 1σ uncertainty) and inventories. The purple line shows the global emissions estimates from
 605 EDGAR (v4.2), the red line shows the emissions reported to the UNFCCC and the green line
 606 shows emissions calculated from all data reported to UNFCCC, including allowance for the
 607 HFC-152a component of unspecified emissions.

608
 609 The data shown in column 3 of Table 2 are the totals of submissions by the national
 610 governments to the UNFCCC (Rio Convention) as reported in Table 2(II) s1 in the Common
 611 Reporting Format (CRF), available on the UNFCCC website (http://unfccc.int/national-reports/annex_ghg_inventories/national_inventories_submissions/items/8108.php). The values
 612 were taken from the 2014 database and cover years 1995, the baseline year for submissions,
 613 to 2012. In addition to reporting calculated emissions of HFCs 23, 32, 125, 134a, 143a, 152a,
 614 227ea, 236fa, 245ca and 43-10mee, individually, many countries also included "unspecified"
 615 emissions in this database (as the sum of their CO₂ equivalents). Where the unspecified
 616 component was small in relation to the national specified emissions, it was disaggregated by
 617 assuming that it had the same fractional contribution of each HFC as reported in the specified
 618 components (adjusted for their CO₂ equivalence). However, in the US, although values of
 619 emissions of several HFCs are calculated specifically for the individual substances, HFCs
 620 152a, 227ea, 245ca and 43-10mee are shown in the database as "commercially confidential"
 621 and their emissions apparently constitute the substantial aggregated "unspecified" emissions
 622 reported. Hence, for the US, these unspecified annual emissions were divided only between
 623 HFCs 152a, 227ea, 245ca and 43-10mee, assuming the same ratio as their reported global
 624 emissions, all expressed as CO₂ equivalents. The values shown in column 4 of Table 2 are the
 625

626 global totals of HFC-152a after adjusting in these ways for the quantities included in
627 “unspecified” emissions.

628 The additional component of US emissions makes a substantial contribution to the
629 very large difference between the UNFCCC data as reported and the adjusted values. This is
630 partly due to the low global warming potential of HFC-152a (a factor of 10 lower than other
631 HFCs) which magnifies its mass component in the 8200 Gg CO₂ equivalent of US
632 “unspecified” emissions.

633 The AGAGE observation based global emissions are substantially higher than the
634 emissions calculated from the UNFCCC GHG reports (2014 submission). It is not
635 unreasonable that UNFCCC-reported emissions are lower than the AGAGE global emission
636 estimates, since countries and regions in Asia (e.g. China, Indonesia, Korea, Malaysia, the
637 Philippines, Taiwan, Vietnam), the Indian sub-continent (e.g. India, Pakistan), the Middle
638 East, South Africa and Latin America do not report to the UNFCCC. Where we include the
639 HFC-152a component of unspecified emissions (green line in Figure 7) results are consistent
640 within the error bars until approximately 2003 to 2005 when they start to diverge (UNFCCC
641 + ‘unspecified’ lower). From 1996-2002, estimated emissions from EDGAR (v4.2) are
642 generally consistent with AGAGE emissions, but then begin to diverge with EDGAR
643 emissions 22 Gg below 2008 AGAGE emissions, the last year for which EDGAR reports
644 emissions.

645

646 *5.2 Regional Emissions of HFC-152a Inferred for Europe, United States, Asia* 647 *and Australia*

648

649 Lunt et al. (2015) have reported global and regional emissions estimates for the most
650 abundant HFCs, based on inversions of atmospheric mole fraction data, aggregated into two
651 categories; those from Annex 1 countries and those from non-Annex 1 countries. The
652 inversion methodology used the NAME model to simulate atmospheric transport close to the
653 monitoring sites, and the Model for Ozone and Related chemical Tracers (MOZART,
654 Emmons et al., 2010) to simultaneously calculate the effect of changes to the global
655 emissions field on each measurement site. The model sensitivities were combined with a
656 prior estimate of emissions (based on EDGAR) and the atmospheric measurements, in a
657 hierarchical Bayesian inversion (Ganesan et al., 2014), to infer emissions.

658 Using this method we infer emissions estimates for the entire world, Europe, North
659 America and East Asia. Table 3 lists our estimated regional emissions in Gg/yr averaged

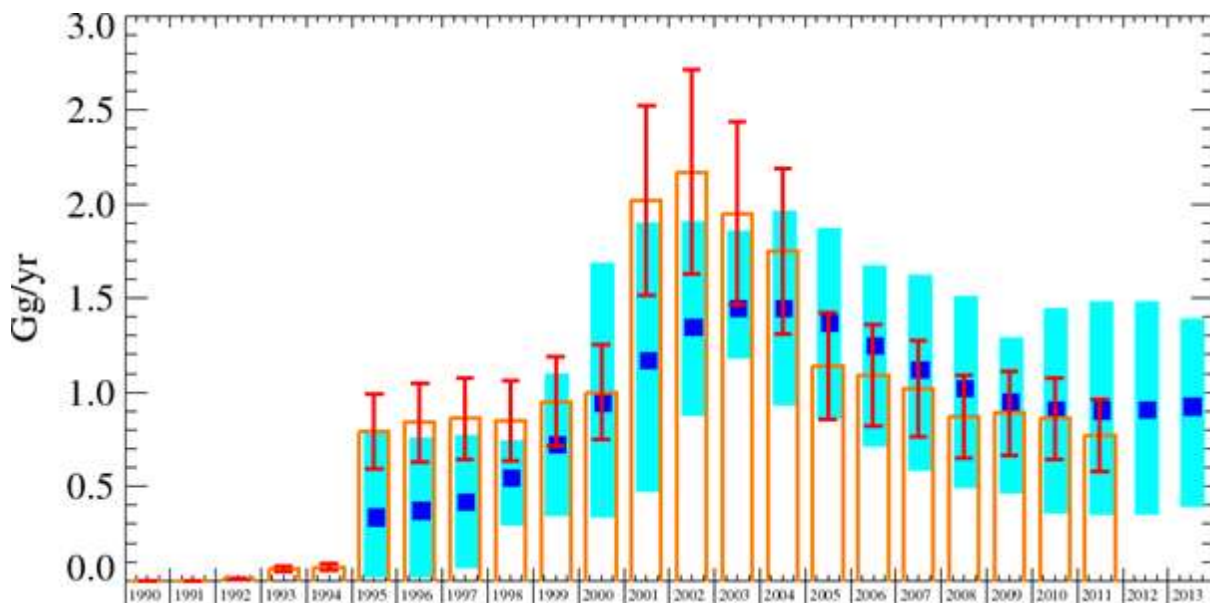
660 across two time periods: 2007–2009 and 2010–2012, together with our global emission
661 estimates averaged over the same time periods from the 12-box model. It is apparent that
662 North American average annual emissions (~30 Gg) are the major contributor to the global
663 total with Europe contributing annual average emissions from about 5–6 Gg/yr. East Asia and
664 Europe contribute emissions of ~7 Gg/yr and ~6 Gg/yr, respectively to the global total. The
665 2007–2009 North American emission estimate of 28 Gg/yr agrees within the uncertainties of
666 HFC-152a emission estimates reported in Barletta et al. (2011) and Simmonds et al. (2015).
667 The North American estimate indicates one reason why the UNFCCC reported amount
668 appears to be so low; more than half the global emissions appear to come from this
669 continental region, yet the UNFCCC reports do not include specific HFC-152a emissions
670 from the US.

671 *5.2.1 InTEM North-West Europe (NWEU) estimated emissions from Mace Head observations*

672
673 The HFC-152a perturbations above baseline, observed at Mace Head, are driven by
674 emissions on regional scales that have yet to be fully mixed on the hemisphere scale. The
675 Mace Head observations are coupled with NAME model air history maps using the inversion
676 system InTEM to estimate surface emissions across NWEU (Manning et al., 2011). NWEU is
677 defined as United Kingdom, Ireland, Germany, France, Benelux and Denmark.

678 As shown in Fig. 8, the NWEU emission estimates for HFC-152a from InTEM (rolling 3-yr
679 averages) agree to within inversion uncertainties with the UNFCCC data (2013 submission)
680 for most years. The estimates of NWEU emissions grew steadily from 1995 reaching a
681 maximum emission of 1.6 ± 0.21 Gg/yr in 2003 with a subsequent decline to 0.98 ± 0.34
682 Gg/yr in 2013.

683
684
685
686
687
688
689
690
691
692



693

694 Figure 8: Emission (Gg/yr) estimates for HFC-152a from North-West Europe. The blue
 695 uncertainty bars represent the 5th and 95th percentiles of the InTEM estimates (rolling 3-yr
 696 averages). The orange bars and associated uncertainty are the UNFCCC inventory estimates
 697 for the NWEU region. (25% uncertainty is estimated by the UK in their National Inventory
 698 Report (NIR) submission to the UNFCCC, the same uncertainty was assumed for North-West
 699 Europe given the lack of additional information).

700

701 *5.2.2 European estimated emissions from European observations at Mace Head*
 702 *Jungfraujoch and Mt. Cimone*

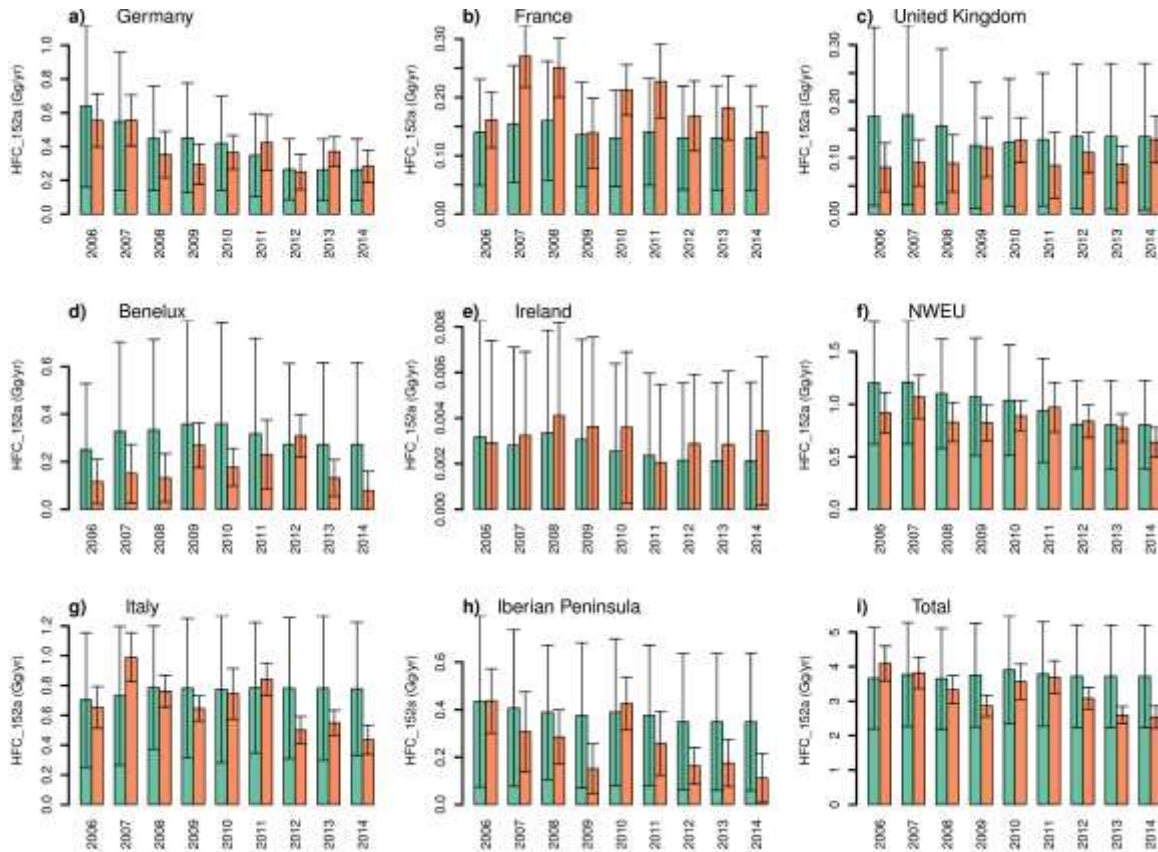
703

704

The temporal evolution of emission estimates for different European regions are given
 705 in Figure 9. In contrast to the InTEM estimates the Bayesian inversion derived emissions in
 706 NWEU were slightly smaller than the UNFCCC estimate and showed a continued decrease
 707 until 2014. Total emissions in the inversion domain ranged from 4 ± 0.5 Gg/yr (2σ
 708 confidence range) for 2006 to only 2.5 ± 0.2 Gg/yr in 2014. This is considerably smaller than
 709 the European Annex I estimate given in section 5.2, but covers a significantly smaller
 710 geographical region. The estimate given in section 5.2 encompassed all countries in Europe
 711 extending beyond the bounds of the area indicated in Fig. 1 (red box). The steady decline in
 712 emissions was interrupted by a local maximum in the years 2010–2012, when emissions
 713 reached 3.6 ± 0.5 (Gg/yr). A minimum in the posterior emissions can be seen in 2009 and was
 714 most pronounced for the Iberian Peninsula, Italy, France and Germany, which might indicate
 715 the influence of the European recession in 2008–2009. For NWEU the emission estimate
 716 remains slightly below the UNFCCC estimates and those estimated by InTEM, but support
 717 the declining trend in European emissions. Despite the fact that Italy does not report HFC-
 718 152a emissions to the UNFCCC, the largest by country emissions were estimated for Italy

719 (up to 1 Gg/yr in 2007). However, a strong decline in these emissions after 2011 was
 720 established here. Similar values for Italian HFC-152a emissions were reported by Brunner et
 721 al. (2012) using observations from Jungfraujoch and Mace Head (but not Mt. Cimone) in an
 722 extended Kalman Filter inversion.

723



724
 725 Figure 9: HFC-152a emission estimates for different European regions using the Bayesian
 726 regional inversion (orange bars) and prior estimates as reported to UNFCCC (green bars).
 727 Error bars indicate 2σ confidence levels. Total prior uncertainties were set to 20% of the total
 728 domain emissions, which may result in different levels of relative uncertainty for each
 729 country/region. Note that prior estimates for Italy were taken from EDGAR instead. Prior
 730 values for 2012 were repeated for each region after 2012.

731

732 *5.2.3 US estimated emissions.*

733

734 Estimates of North American emissions have been reported by several groups (see
 735 also estimates from this study in Table 3). Millet et al. (2009) report average US emissions
 736 for 2004-2006 of 7.6 Gg (4.8-10 Gg) compared with the UNFCCC average 2005-2006
 737 estimate of 12.3 Gg calculated from UNFCCC data. Miller et al. (2012) provided HFC-152a
 738 emissions estimates averaged from 2004-2009 of 25 Gg (11-50 Gg). Barletta et al. (2011)
 739 reported a 2008 HFC-152a emission estimate of 32 ± 4 Gg. In a recent investigation of the
 740 surface-to-surface transport of HFC-152a from North America to Mace Head, Ireland, an

741 interspecies correlation method with HFC-125 as the reference gas was also used to estimate
742 North American emissions primarily from the eastern seaboard region. The average 2008
743 HFC-152a emission estimate was 31.3 ± 5.9 Gg (Simmonds et al., 2015); in very close
744 agreement with the estimate from Barletta et al. (2011). HFC-152a emission estimates for
745 2005 (10.1 Gg) and 2006 (12.5 Gg) reported by Stohl et al. (2009) are close to the
746 (recalculated) UNFCCC estimates in those years.

747 If the sources of emissions from the US were solely technical aerosols and
748 construction foam, emissions would be expected to be far lower. These were the historic
749 uses in Europe and Japan and resulted in emissions ten times less than those estimated
750 for the US. However, in the US, do-it-yourself (DIY) refilling of car air conditioners is not
751 only permitted but thriving (Zhan et al., 2014), with an estimated 24 million DIY
752 refilling operations attempted each year. The practice is banned in Europe (OJ., 2014).
753 Furthermore, there is ample evidence online that HFC-152a is extensively used in DIY
754 refilling on account of its lower cost. It is a technically suitable replacement for HFC-134a,
755 although there are safety concerns of importance to vehicle manufacturers (Hill., 2003). If the
756 quantities estimated by Zhan et al. 2014 were met using HFC-152a diverted from the retail
757 trade in technical aerosols, some 10 to 20 Gg/yr of HFC-152a could be released into the
758 atmosphere from this source alone.

759

760 *5.2.4 East Asian emissions*

761

762 Emissions of HFC-152a from China were estimated to be 4.3 ± 2.3 Gg/yr in 2004-
763 2005 (Yokouchi et al., 2006), 3.4 ± 0.5 Gg/yr in 2008 (Stohl et al., 2010) and 5.7 (4.3-7.6)
764 Gg/yr in 2008 (Kim et al., 2010). Li et al. (2011) using an interspecies correlation method
765 also reported emission estimates for East Asia (China, South Korea and Taiwan, with HCFC-
766 22 as the reference tracer) and Japan (reference tracer HFC-134a) for the period between
767 November 2007 and December 2008. For China, emissions were estimated to be 5.4 (4-7.4)
768 Gg/yr. In contrast the Taiwan region Korea and Japan had lower estimated emissions totalling
769 1.39 Gg/yr. These estimates are within the uncertainties of our East Asia emissions reported
770 in section 5.2 and Table 3.

771 Yao et al. (2012), using the interspecies correlation method with carbon monoxide as
772 the reference tracer, reported more recent Chinese emissions of 2 ± 1.8 Gg/yr in 2010-2011.
773 This would imply some reduction in Chinese emissions compared with earlier years.

774

775 5.2.5 Australian HFC-152a emissions from Cape Grim data

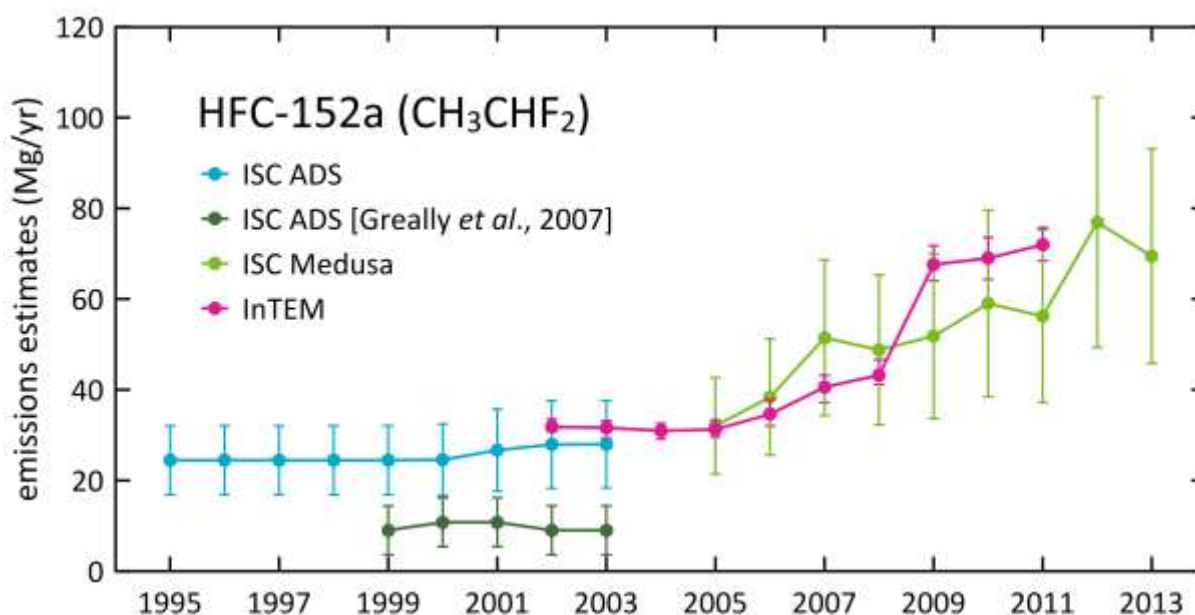
776

777 SE Australian emissions of HFC-152a are estimated using the positive enhancements
778 above baseline or background concentrations observed at Cape Grim using interspecies
779 correlation with CO as the reference species (ISC: Dunse et al., 2005; Greally et al., 2007)
780 and inverse modelling (InTEM: Manning et al., 2003, 2011). Figure 2a (CGO) shows an
781 overall increase in the magnitude of HFC-152a pollution episodes, presumably due to
782 increasing regional emissions. Detailed analysis of these pollution episodes using air mass
783 back trajectories shows clearly that the HFC-152a pollution seen at Cape Grim originates
784 largely from Melbourne and the surrounding Port Phillip region.

785 Australian HFC-152a emissions of 5-10 Mg/yr via interspecies correlation (ISC) have
786 been reported for the period 1998-004, although it was noted that these emission estimates
787 were near the detection limit of the ISC method (Greally et al., 2007). Recently, significant
788 improvements have been made to this ISC method, including a revised (upward) CO
789 emissions inventory for the Melbourne/Port Phillip region, exclusion of high CO events in the
790 Cape Grim in situ CO record, resulting from CO emissions from biomass burning and coal
791 combustion in the Latrobe Valley (east of Port Phillip) and a revised (upward) population-
792 based scaling factor (5.4), used to convert Melbourne/Port Phillip emissions to Australian
793 emissions (Fraser et al., 2014a, b). Each of these changes to the ISC method resulted in
794 higher trace gas emission estimates. The revised (compared to Greally et al., 2007) Australian
795 HFC-152a emission estimates from the ISC method are shown in the 2nd column of Table 4
796 and in Figure 10 as 3-year running averages.

797 The InTEM model (Manning et al., 2003, 2011) has been used to derive HFC-152a
798 emissions from Victoria/Tasmania (Fraser et al., 2014a). Annual Australian emissions are
799 calculated from Victoria/Tasmania emissions using a population based scale factor of 3.7 and
800 are shown in Figure 10 and the 3rd column of Table 4, interpolated from rolling 3-year
801 emission estimates. Over the period 2002-2011, the average Australian HFC-152a emissions
802 from ISC and InTEM agree to within 2%. The method for estimating the InTEM
803 uncertainties are discussed above. No additional uncertainty was applied to the estimates
804 through the process of up-scaling from Victoria/Tasmania to Australian totals. The
805 assumption was made that the use of HFC-152a per head of population was identical across
806 Australia as we have no more detailed information.

807



808

809 Figure 10. Australian HFC-152a emissions (Mg/yr) calculated from Cape Grim *in situ*
 810 observations via ISC, using ADS and Medusa data, and inverse modelling using InTEM
 811 (Medusa data). Australian emissions are derived from SE Australian emissions, scaled by
 812 population (see text). Uncertainties are 25th-75th percentiles (InTEM) and 1 s.d. (ISC).

813 Australian HFC-152a emissions have increased steadily from 25 Mg/yr in the late-
 814 1990s to over 60 Mg/yr in the late-2000s. The 2012 and 2013 emissions have been estimated
 815 from Cape Grim data by ISC at 77 and 69 Mg, respectively. Australian HFC-152a emissions
 816 (1998-2004) are 25-30 Mg, significantly higher than estimated (5-10 Mg/yr) in Greally et al.
 817 (2007), resulting from improvements in the ISC method (see above).

818 Compared to the global values derived above, Australian emissions are 0.1% of global
 819 emissions based on ISC/InTEM data. It is unusual for Australian emissions of an industrial
 820 chemical to be as low as 0.1% of global emissions. For other HFCs, CFCs and HCFCs (for
 821 example HFC-134a, CFC-12, HCFC-22), Australian emissions as fraction of global
 822 emissions are typically 1-2%, similar to Australia's fraction of global gross domestic product
 823 (GDP, 1.9%, 2014) but significantly larger than Australia's fraction of global population
 824 (0.33%, 2014) (Fraser et al., 2014b).

825 The possible reasons for the low Australian HFC-152a emissions (relatively low use
 826 in Australia compared to rest of world) are being investigated. One suggestion (M. Bennett,
 827 Refrigerant Reclaim Australia, personal communication, 2013) is that a significant major-
 828 volume use in other parts of the world for HFC-152a is as an aerosol propellant, a use not
 829 taken up to any significant degree in Australia.

830 6. Conclusions

831 Atmospheric abundances and temporal trends of HFC-152a have been estimated from
832 data collected at the network of eleven globally-distributed monitoring sites. The longest
833 continuous in situ record at Mace Head, Ireland covers a 20-year period from 1994-2014.
834 Other stations within the network have observational records from 9-16 years, with only a
835 short record (2010–2012) at Shangdianizi, China. From selected baseline in situ
836 measurements and measurements of archived air samples dating back to 1978 the long-term
837 growth rate of HFC-152a has been deduced. Analysing the enhancements above baseline
838 coupled with atmospheric transport models permitted us to estimate both regional and global
839 HFC-152a emissions. However, it should be noted that the various models use different
840 domains to obtain regional emissions estimates.

841 The annual average NH (Mace Head + Trinidad Head) baseline mole fraction in 1994
842 was 1.2 ppt reaching an annual average mole fraction of 10.1 ppt in 2014. In the SH (Cape
843 Grim) the annual average mole fraction increased from 0.84 ppt in 1998 to 4.5 ppt in 2014.
844 Using the global average mole fraction obtained from the AGAGE 12-box model we estimate
845 that the HFC-152a contribution to radiative forcing was 0.61 ± 0.02 mW/m² in 2014. Since
846 the first in situ measurements in 1994 the global annual growth rate of HFC-152a has
847 increased to a maximum annual growth rate in 2006 of 0.81 ± 0.05 ppt/yr. More recently the
848 average annual growth rate has slowed to 0.38 ± 0.04 ppt/yr in 2010, and become negative,
849 with a growth rate in 2013-2014 of minus 0.06 ± 0.05 ppt/yr.

850 Global HFC-152a emissions increased from 7.3 ± 5.6 Gg/yr in 1994 to 52.5 ± 20.15
851 Gg/yr in 2014. Global emissions are dominated by emissions from North America with this
852 region being responsible for ~67% of global emissions in our estimates. Estimates of north-
853 western European emissions of ~0.9 Gg/yr, (2010-2012 average) agree within the
854 uncertainties for the two regional models (see sections 3.3 and 3.4) and overlap with the
855 UNFCCC inventory. For the combined Eulerian and Lagrangian models (see 3.2 and Table
856 3), that encompass all European countries, we derive a 2010-2012 average emission of 5.2
857 Gg/yr. East Asian countries contribute 1 Gg/yr (Annex 1) and 6 Gg/yr (Non-Annex 1) to the
858 global total (2010-2012 averages). All of the models studies indicate a current declining trend
859 in European and Asian emissions.

860 Substantial differences in emission estimates of HFC-152a were found between this
861 study and those reported to the UNFCCC which we suggest arises from underestimated North
862 American emissions and undeclared Asian emissions; reflecting the incomplete global

863 reporting of GHG emissions to the UNFCCC and/or biases in the accounting methodology.
864 Ongoing, continuous, and accurate globally and regionally distributed atmospheric
865 measurements of GHGs, such as HFC-152a, are required for ‘top-down’ quantification of
866 global and regional emissions of these gases, thereby enabling improvements in national
867 emissions inventories, or ‘bottom-up’ emissions data collected and reported to the UNFCCC
868 (Weiss and Prinn, 2011).

869

870 **Data availability**

871 The entire ALE/GAGE/AGAGE data base comprising every calibrated measurement
872 including pollution events is archived on the Carbon Dioxide Information and Analysis
873 Center (CDIAC) at the U.S. Department of Energy, Oak Ridge National Laboratory.

874 **Acknowledgements**

875

876 We specifically acknowledge the cooperation and efforts of the station operators (G.
877 Spain, MHD; R. Dickau, THD; P. Sealy, RPB; NOAA officer-in-charge, SMO) at the
878 AGAGE stations and all other station managers and support staff at the different monitoring
879 sites used in this study. We particularly thank NOAA and NILU for supplying some of the
880 archived air samples shown, allowing us to fill important gaps. The operation of the AGAGE
881 stations was supported by the National Aeronautic and Space Administration (NASA, USA)
882 (grants NAG5-12669, NNX07AE89G and NNX11AF17G to MIT; grants NAG5-4023,
883 NNX07AE87G, NNX07AF09G, NNX11AF15G and NNX11AF16G to SIO); the Department
884 of the Energy and Climate Change (DECC, UK) (contract GA0201 to the University of
885 Bristol); the National Oceanic and Atmospheric Administration (NOAA, USA) (contract
886 RA133R09CN0062 in addition to the operations of American Samoa station); and the
887 Commonwealth Scientific and Industrial Research Organisation (CSIRO, Australia), Bureau
888 of Meteorology (Australia). Financial support for the Jungfraujoch measurements is
889 acknowledged from the Swiss national programme HALCLIM (Swiss Federal Office for the
890 Environment (FOEN). Support for the Jungfraujoch station was provided by International
891 Foundation High Altitude Research Stations Jungfraujoch and Gornergrat (HFSJG). The
892 measurements at Gosan, South Korea were supported by the Basic Science Research Program
893 through the National Research Foundation of Korea (NRF) funded by the Ministry of
894 Science, ICT & Future Planning (2014R1A1A3051944). Financial support for the Zeppelin
895 measurements is acknowledged from the Norwegian Environment Agency. Financial support

896 for the Shangdianzi measurements is acknowledged from the National Nature Science
897 Foundation of China (41030107, 41205094). The CSIRO and the Australian Government
898 Bureau of Meteorology are thanked for their ongoing long-term support of the Cape Grim
899 station and the Cape Grim science program. M. Rigby is supported by a NERC Advanced
900 Fellowship NE/I021365/1.

901 **References.**

902
903 Archibald, A.T., Witham, C.S., Ashfold, M.J., Manning, A.J., O'Doherty, S., Grealley, B.R.,
904 Young, D., and Shallcross D.E.: Long-term high frequency measurements of ethane, benzene
905 and methyl chloride at Ragged Point, Barbados: Identification of long-range transport events,
906 *Elementa: Science of the Anthropocene*, 3, 000068, doi:10.12952/journal.elementa.000068,
907 2015.

908 | Arnold, T., Mühle, J., Salameh, P. K., Harth, C. M., Ivy, D. J., and Weiss, R. F.: Automated
909 measurement of nitrogen trifluoride in ambient air, *Anal. Chem.*, 84, 4798–4804, 2012.

910
911 Ashford, P., Clodic, D., McCulloch, A and L. Kuijpers .: Emission profiles from the foam
912 and refrigeration sectors comparison with atmospheric concentrations. Part 2: Results and
913 discussion, *Int. J. Refrigeration.*, 27(7), 701– 716, 2004.

914
915 Barletta, B., Nissenson, P., Meinardi, S., Dabdub, D., Sherwood Rowland, F., VanCuren,
916 R.A., Pederson, J., Diskin, G.S., and D.R. Blake, D.R.: HFC-152a and HFC-143a emission
917 estimates and characterization of CFCs, CFC replacements and other halogenated solvents
918 measured during the 2008 ARCTAS campaign (CARB phase) over the South Coast Air
919 Basin of California. *Atmos. Chem. Phys.*, 2655-2669, 2011.

920 Brunner, D., Henne, S., Keller, C. A., Reimann, S., Vollmer, M. K., O'Doherty, S., and
921 Maione, M.: An extended Kalman-filter for regional scale inverse emission estimation,
922 *Atmos. Chem. Phys.*, 12, 3455-3478, doi: 10.5194/acp-12-3455-2012, 2012.

923
924 Cunnold, D. M., R.G. Prinn, R.G., Rasmussen, R., Simmonds, P.G., Alyea, F.N., Cardlino,
925 C., Crawford, A.J., Fraser, P.J., and R. Rosen.: The lifetime atmospheric experiment, III:
926 lifetime methodology and application to three years of CFCl_3 data, *J. Geophys. Res.*, 88,
927 8379-8400, 1983.

928 Cunnold, D. M., Fraser, P.J., Weiss, R.F., Prinn, R.G., Simmonds, P.G., Miller, B.R., Alyea,
929 F.N., Crawford, A.J., and Rosen, R.: Global trends and annual releases of CCl_3F and CCl_2F_2
930 estimated from ALE/GAGE and other measurements from July 1978 to June 1991, *J.*
931 *Geophys. Res.*, 99, 1107-1126, 1994.

932
933 DoE, National Inventory Report 2012, Volume 1, Australian Government Department of the
934 Environment, April 2014, 351 pp, 2014.

935

936 Dunse, B., Steele, P., Fraser, P., and Wilson, S.: An analysis of Melbourne pollution episodes
937 observed at Cape Grim from 1995-1998, In: *Baseline Atmospheric Program (Australia)*
938 *1997-98*, N. Tindale, R. Francey & N. Derek (eds.), Bureau of Meteorology and CSIRO
939 Atmospheric Research, Melbourne, Australia, 34-42, 2001.

940 Dunse, B.: Investigation of urban emissions of trace gases by use of atmospheric
941 measurements and a high-resolution atmospheric transport model. PhD thesis, Wollongong
942 University, Wollongong, NSW, Australia, 2002.

943

944 Dunse, B., P. Steele, S. Wilson, P. Fraser & P. Krummel, (2005). Trace gas emissions from
945 Melbourne Australia, based on AGAGE observations at Cape Grim, Tasmania, 1995-2000,
946 *Atmos. Environ.*, 39, 6334-6344.

947

948 EC-JRC/PBL.: Emission Database for Global Atmospheric Research (EDGAR),
949 version 4.2, European Commission, Joint Research Centre (JRC)/Netherlands Environmental
950 Assessment Agency (PBL). [<http://edgar.jrc.ec.europa.eu>], 2011.

951

952 Emmons, L.K., Walters, S., Hess, P.G., Lamarque, J.F., Pfister, G.G., Fillmore, D., Granier,
953 C., Guenther, A., Kinnison, D., Leapple, T., Orlando, J., Tie, X., Tyndall, G., Wiedinmyer,
954 C., Baughcum, S.L., and Kloster, S.: Description and evaluation of the Model for Ozone and
955 Related chemical Tracers, version 4 (MOZART-4), *Geosci. Model Dev.*, 3, 43–67,
956 doi:10.5194/gmd-3-43, 2010.

957

958 Forster, P., Ramaswamy, V., Artaxo, P., Berntsen, T., Betts, R., Fahey, D. W., Haywood, J.,
959 Lean, J., Lowe, D. C., Myhre, G., Nganga, J., Prinn, R., Raga, G., Schulz, M., and Van
960 Dorland, R.: Changes in atmospheric constituents and in radiative forcing, in: *Climate*
961 *Change (2007): The Physical Science Basis. Contribution of Working Group I to the Fourth*
962 *Assessment Report of the Intergovernmental Panel on Climate Change*, ed.by: Solomon, S.
963

964 Fraser, P., Dunse, B., Krummel, P., Steele, P., and Derek, N.: Australian HFC, PFC, Sulphur
965 Hexafluoride & Sulphuryl Fluoride Emissions, Australian Government Department of the
966 Environment, 28pp, 2014a.

967 Fraser, P., Dunse, B., Manning, A. J., Wang, R., Krummel, P., Steele, P., Porter, L., Allison,
968 C., O'Doherty, S., Simmonds, P., Mühle, J., and R. Prinn.: Australian carbon tetrachloride
969 (CCl₄) emissions in a global context, *Environ. Chem.*, 11, 77-88, 2014b.

970

971 Ganesan, A. L., Rigby, M., Zammit-Mangion, A., Manning, A. J., Prinn, R. G., Fraser, P. J.,
972 Harth, C. M., Kim, K.-R., Krummel, P. B., Li, S., Mühle, J., O'Doherty, S., Park, S.,
973 Salameh, P. K., Steele, L. P., and Weiss, R. F.: Characterization of uncertainties in
974 atmospheric trace gas inversions using hierarchical Bayesian methods, *Atmos. Chem. Phys.*,
975 14, 3855-3864, doi:10.5194/acp-14-3855-2014, 2014.

976

977 Grealley, B. R., Manning, A. J., Reimann, S., McCulloch, A., Huang, J., Dunse, B. L.,
978 Simmonds, P. G., Prinn, R. G., Fraser, P. J., Cunnold, D. M., O'Doherty, S., Porter, L. W.,
979 Stemmler, K., Vollmer, M. K., Lunder, C. R., Schmidbauer, N., Hermansen, O., Arduini, J.,
980 Salameh, P. K., Krummel, P. B., Wang, R. H. J., Folini, D., Weiss, R. F., Maione, M.,

981 Nickless, G., Stordal, F., and R. G. Derwent.: Observations of 1,1-difluoroethane (HFC-152a)
982 at AGAGE and SOGE monitoring stations in 1994-2004 and derived global and regional
983 emission estimates, *J. Geophys. Res.*, 112, D06308, doi:10.1029/2006JD007527, 2007.
984

985 Hill W.R.: HFC152a as the alternative refrigerant, available at
986 <http://ec.europa.eu/environment/archives/mac2003/pdf/hill.pdf>, 2003.
987

988 IPCC/TEAP.: Progress Report-Volume-1-May 2011. Technology and Assessment Panel.
989 United Nations Environment Programme, Ozone Secretariat, P.O. Box 30552, Nairobi,
990 Kenya, 2011.
991

992 Keller, C. A., Hill, M., Vollmer, M. K., Henne, S., Brunner, D., Reimann, S., O'Doherty, S.,
993 Arduini, J., Maione, M., Ferenczi, Z., Haszpra, L., Manning, A. J., and Peter, T.: European
994 Emissions of Halogenated Greenhouse Gases Inferred from Atmospheric Measurements,
995 *Environ. Sci. Technol.*, 46, 217-225, doi: 10.1021/es202453j, 2012.
996

997 Kim, J., Li, S., Kim, K-R., Stohl, A., Mühle, J., Kim, S-K., Park, M-K., Kang, D-J., Lee, G.,
998 Harth, C.M., Salameh, P.K. and Weiss, R.F.: Regional emissions determined from
999 measurements at Jeju Island, Korea: Halogenated compounds from China. *Geophys. Res.*
1000 *Lett.*, 37, doi:10.1029/2010GL043263, 2010.
1001

1002 Krummel, P. B., Langenfelds, R.L., Fraser, P.J., Steele, L.P., and L.W. Porter.: Archiving of
1003 Cape Grim air, in *Baseline Atmospheric Program, Australia 2005-2006, 2007*. edited by;
1004 Cainey, J.M., N. Derek and P.B. Krummel., Australian Bureau of Meteorology and CSIRO
1005 Marine and Atmospheric Research, Melbourne, Australia, 55-57, 2007.
1006

1007 Krummel, P. B., Fraser, P. Steele, P., Derek, N., Rickard, C., Ward, J., Somerville, N.,
1008 Cleland, S., Dunse, B., Langenfelds, R., Baly S., and Leist, M.: The AGAGE *in situ* program
1009 for non-CO₂ greenhouse gases at Cape Grim, 2009-2010, *Baseline Atmospheric Program*
1010 *(Australia) 2009-2010*, N. Derek P. Krummel & S. Cleland (eds.), Australian Bureau of
1011 Meteorology and CSIRO Marine and Atmospheric Research, Melbourne, Australia, 55-70,
1012 2014.
1013

1014 Langenfelds, R.L., Fraser, P.J., Francey, R.J., Steele, L.P., Porter, L.W., and Allison, C.E.:
1015 The Cape Grim Air Archive; the first seventeen years, 1978-1995, in; *Baseline Atmospheric*
1016 *Program, Australia 1994-1995*, edited by; Francey, R.J., A.L. Dick and N. Derek., Bureau of
1017 Meteorology and CSIRO Division of Atmospheric Research, Melbourne, 53-70, 1996.
1018

1019 Li, S., Kim, J., Kim, K.-R., Mühle, J., Kim, S.-K., Park, M.-K., Stohl, A., Kang, D.-J.,
1020 Arnold, T., Harth, C. M., Salameh, P. K., and Weiss, R. F.: Emissions of halogenated
1021 compounds in East Asia determined from measurements at Jeju Island, Korea, *Environ.*
1022 *Sci. Technol.*, 45, 5668–5675, doi:10.1021/es104124k, 2011.
1023

1024 Lunt, M.F., Rigby, M., Ganesan, A. L., Manning, A.J., Prinn, R.G., O'Doherty, S., Mühle, J.,
1025 Harth, C.M., Salameh, P.K., Arnold, T., Weiss, R.F., Saito, T., Yokouchi. Y., Krummel, P.B.,
1026 Steele, L.P., Fraser, P.J., Li, S., Park, S., Reimann, S., Vollmer, M.K., Lunder, C.,
1027 Hermansen, O., Schmidbauer, N., Maione, M., Young, D., and Simmonds, P.G.: Reconciling

1028 reported and unreported HFC emissions with atmospheric observations, PNAS, 112, 5927-
1029 5931, doi/10.1073/pnas.1420247112, 2015.

1030

1031 Maione, M., Graziosi, F., Arduini, J., Furlani, F., Giostra, U., Blake, D.R., Bonasoni, P.,
1032 Fang, X., Montzka, S.A., O'Doherty, S.J., Reimann, S., Stohl, A., and Vollmer, M.K.:
1033 Estimates of European emissions of methyl chloroform using a Bayesian inversion method.
1034 Atmos. Chem. Phys., 14, 9755-9770, 2014, doi:10.5194/acp-14-9755, 2014.

1035

1036 Manning, A.J., Ryall, D., Derwent, R., Simmonds, P., and O'Doherty, S.: Estimating
1037 European ozone depleting and greenhouse gases using observations and a modelling
1038 attribution technique, J. Geophys. Res., 108, 4405, doi:10.1029/2002JD002312, 2003.

1039

1040 Manning, A.J., O'Doherty, S., Jones, A.R., Simmonds, P.G., and Derwent, R.G.: Estimating
1041 UK methane and nitrous oxide emissions from 1990 to 2007 using an inversion modelling
1042 approach, J. Geophys. Res., 116, D02305, doi:10.1029/2010JD004763, 2011.

1043

1044 Manning, A.J., and Weiss, R.F.: Quantifying Regional GHG Emissions from Atmospheric
1045 Measurements: HFC-134a at Trinidad Head, 50th anniversary of the Global Carbon Dioxide
1046 Record Symposium and Celebration, Kona, Hawaii, available at:
1047 http://www.esrl.noaa.gov/gmd/co2-conference/pdfs/quantifying_abstract.pdf (last
1048 2010), 2007.

1049

1050 McCulloch, A.: Evidence for improvements in containment of fluorinated hydrocarbons
1051 during use: an analysis of reported European emissions, Environ. Sci. Policy., 12, 149–156,
1052 doi:10.1016/j.envsci.2008.12.003, 2009.

1053

1054 Miller, B., Weiss, R., Salameh, P., Tanhua, T., Grealley, B., Muhle, J., and Simmonds, P.:
1055 Medusa: a sample pre-concentration and GC-MS detector system for *in situ* measurements of
1056 atmospheric trace halocarbons, hydrocarbons and sulphur compounds, Anal. Chem., 80,
1057 1536-1545, 2008.

1058

1059 Miller, B. R., Rigby, M., Kuijpers, L. J. M., Krummel, P. B., Steele, L. P., Leist, M., Fraser,
1060 P. J., McCulloch, A., Harth, C., Salameh, P., Mühle, J., Weiss, R. F., Prinn, R. G., Wang, R.
1061 H. J., O'Doherty, S., Grealley, B. R., and Simmonds, P. G., : HFC-23 (CHF₃) emission trend
1062 response to HCFC-22 (CHClF₂) production and recent HFC-23 emission abatement
1063 measures, Atmos Chem. Phys., 10, 7875–7890, doi:10.5194/acp-10-7875, 2010.

1064

1065 Miller, J. B., Lehman, S.J., Montzka, S.A., Sweeney, C., Miller, B.R., Karion, A., Wolak, C.,
1066 Dlugokencky, E.J., Southon, J., Turnbull, J. C., Tans, P. P.: Linking emissions of fossil fuel
1067 CO₂ and other anthropogenic trace gases using atmospheric ¹⁴CO₂. J. of Geophys Res., 117,
1068 D08302, doi:10.1029/2011JD017048, 2012.

1069 Millet, D.B., Atlas, L.E., Blake, D.R., Blake, N.J., Diskin, C.S., Holloway, J.D., Hudman,
1070 R.C., Meinardi, S., Ryerson, T.B., Sachse, G.W.: Halocarbon emissions from the United
1071 States and Mexico and their Global warming potential. Environ. Sci. Technol., 43(4), 1055-
1072 1060, doi 10.1021/Es802146j, 2009.

1073

1074 Mühle, J., Ganesan, A. L., Miller, B. R., Salameh, P. K., Harth, C. M., Grealley, B. R., Rigby,
1075 M., Porter, L. W., Steele, L. P., Trudinger, C. M., Krummel, P. B., O'Doherty, S., Fraser, P.
1076 J., Simmonds, P. G., Prinn, R. G., and Weiss, R. F.: Perfluorocarbons in the global

1077 atmosphere: tetrafluoromethane, hexafluoroethane, and octafluoropropane, *Atmos. Chem.*
1078 *Phys.*, 10, 5145–5164, doi:10.5194/acp-10-5145, 2010.

1079
1080 Myhre, G., Shindell, D., Bréon, F.-M., Collins, W., Fuglestedt, J., Huang, J., Koch, D.,
1081 Lamarque, J.-F., Lee, D., Mendoza, B., Nakajima, T., Robock, A., Stephens, G., Takemura,
1082 T., Zhang, H.: Anthropogenic and Natural Radiative Forcing. In: *Climate Change 2013: The*
1083 *Physical Science Basis. Contribution of Working Group I to the Fifth Assessment Report of*
1084 *the Intergovernmental Panel on Climate Change* [Stocker, T.F., D. Qin, G. K. Plattner, M.
1085 Tignor, S.K. Allen, J. Boschung, A. Nauels, Y. Xia, V. Bex and P.M. Midgley (eds.)].
1086 Cambridge University Press, Cambridge, United Kingdom and New York, NY, USA, 2013.

1087 O’Doherty, S., Cunnold, D., Sturrock, G.A., Ryall, D., Derwent, R.G., Wang, R.H.J.,
1088 Simmonds, P., Fraser, P.J., Weiss, R.F., Salameh, P., Miller, B.R., and Prinn, R.G.: In-Situ
1089 Chloroform Measurements at AGAGE Atmospheric Research Stations from 1994 –1998, *J.*
1090 *Geophys. Res.*, 106, No. D17, 20,429-20,444, ISSN: 0747-7309, 2001.

1091 O’Doherty, S., Cunnold, D. M., Miller, B. R., Mühle, J., McCulloch, A., Simmonds, P. G.,
1092 Mühle, J., McCulloch, A., Simmonds, P. G., Manning, A. J., Reimann, S., Vollmer, M. K.,
1093 Grealley, B. R., Prinn, R. G., Fraser, P. J., Steele, L. P., Krummel, P. B., Dunse, B. L., Porter,
1094 L. W., Lunder, C. R., Schmidbauer, N., Hermansen, O., Salameh, P. K., Harth, C. M., Wang,
1095 R. H. J., and Weiss, R. F.: Global and regional emissions of HFC-125 (CHF₂CF₃) from in situ
1096 and air archive atmospheric observations at AGAGE and SOGE observatories, *J. Geophys.*
1097 *Res.*, 114, D23304, doi:10.1029/2009jd012184, 2009.

1098
1099 O’Doherty, S., Rigby, M., Mühle, J., Ivy, D.J., Miller, B. R., Young, D., Simmonds,
1100 P. G., Reimann, S., Vollmer, M. K., Krummel, P. B., Fraser, P. J., Steele, L. P., Dunse, B. L.,
1101 Salameh, P. K., Harth, C. M., Arnold, T., Weiss, R. F., Kim, J., Park, S., Li, S., Lunder, C.,
1102 Hermansen, O., Schmidbauer, N., Zhou, L.X., Yao, B., Wang, R. H. J., Manning, A., and
1103 Prinn, R. G.: Global emissions of JHFC-143a (CH₃CF₂) and HFC-32 (CH₂F₂) from in situ
1104 and air archive atmospheric observations. *Atmos. Chem. Phys.*, 14, (17), 9249-9258,
1105 10.5194/acp-14-9249, 2014.

1106
1107 OJ (Official Journal of the European Union): Regulation (EU) No 517/2014 of the European
1108 Parliament and of the Council of 16 April 2014 on fluorinated greenhouse gases and
1109 repealing Regulation (EC) No 842/2006, Official Journal L 150/195, 2014.

1110
1111 Press, W.H., Teukolsky, S.A., Vetterling, W.T., and Flannery, B.P.: *Numerical Recipes in*
1112 *Fortran: The art of scientific computing*, 2nd edition, Publ. Cambridge University Press, UK,
1113 1992.

1114 Prinn, R., Cunnold, D., Simmonds, P., Alyea, F., Boldi, R., Crawford, A., Fraser, P., Gutzler,
1115 D., Hartlet, D., Rose, R., and Rasmussen, R.: Global average concentration and trend for
1116 hydroxyl radicals deduced from ALE/GAGE trichloroethane (methyl chloroform) data for
1117 1978–1990, *J. Geophys. Res.*, 97, 2445–2461, 1992.

1118
1119 Prinn, R., Weiss, R.F., Fraser, P., Simmonds, P., Cunnold, D., Alyea, F., O’Doherty, S.,
1120 Salameh, P., Miller, B., Huang, J., Wang, R., Hartley, D., Harth, C., Steele, P., Sturrock, G.,
1121 Midgley, P and McCulloch, A.: A history of chemically and radiatively important gases in air
1122 deduced from ALE/GAGE/AGAGE, *J. Geophys. Res.*, 105 (D14): 17751-17792, 2000.

1123
1124 Reimann, S., Schaub, D., Stemmler, K., Folini, D., Hill, M., Hofer, P., Buchmann, B.,
1125 Simmonds, P.G., Grealley, B.R., and O'Doherty, S.: Halogenated greenhouse gases at the
1126 Swiss High Alpine Site of Jungfraujoch (3580 m asl): Continuous measurements and their
1127 use for regional European source allocation, *J. Geophys. Res.*, 109, D05307,
1128 doi:10.1029/2003JD003923, 2004.
1129
1130 Rigby, M., Ganesan, A.L., Prinn, R.G.: Deriving emissions time series from sparse
1131 atmospheric mole fractions, *J. Geophys. Res.*, 116, D08306, doi:10.1029/2010JD015401,
1132 2011a.
1133
1134 Rigby, M., Manning, A.J., Prinn, R.G.: Inversion of long-lived trace gas emissions using
1135 combined Eulerian and Lagrangian chemical transport models, *Atmos. Chem. Phys.* 11,
1136 9887–9898, 2011b.
1137
1138 Rigby, M., Prinn, R. G., O'Doherty, S., Montzka, S. A., McCulloch, A., Harth, C. M., Mühle,
1139 J., Salameh, P. K., Weiss, R. F., Young, D., Simmonds, P. G., Hall, B. D., Dutton, G. S.,
1140 Nance, D., Mondeel, D. J., Elkins, J. W., Krummel, P. B., Steele, L. P., and Fraser, P. J.: Re-
1141 evaluation of the lifetimes of the major CFCs and CH₃CCl₃ using atmospheric trends, *Atmos.*
1142 *Chem. Phys.*, 13, 2691–2702, doi:10.5194/acp-13-269, 2013.
1143
1144 Rigby, M., Prinn, R., O'Doherty, S., Miller, B., Ivy, D., Muhle, J., Harth, C., Salameh, P.,
1145 Arnold, T., Weiss, R., Krummel, P., Steele, P., Fraser, P., Young, D., and Simmonds, P.:
1146 Recent and future trends in synthetic greenhouse gas radiative forcing, *Geophys. Res. Letts.*,
1147 41, 2623-2630, 2014.
1148
1149 Ruckstuhl, A.F., Henne, S., Reimann, S., Steinbacher, M., Vollmer, M.K., O'Doherty, S.,
1150 Buchmann, B., and Hueglin, C.: Robust extraction of baseline signal of atmospheric trace
1151 species using local regression, *Atmos. Meas. Tech.*, 5, 2613-2624, doi:10.5194/amt-5-2613-
1152 2012, 2012.
1153
1154 Ryall, D. B., Derwent, R. G., Simmonds, P.G., and O'Doherty, S.: Estimating source regions
1155 of European emissions of trace gases from observations at Mace Head, *Atmos. Environ.*, 35,
1156 2507–2523, 2001.
1157
1158 Simmonds, P. G., O'Doherty, S., Nickless, G., Sturrock, G.A., Swaby, R., Knight, P.,
1159 Ricketts, J., Woffenden, G., and Smith, R.: Automated gas chromatographic/mass
1160 spectrometer for routine atmospheric field measurements of the CFC replacement
1161 compounds, the hydrofluorocarbons and hydrochlorofluorocarbons, *Anal. Chem.*, 67, 717–
1162 723, 1995.
1163
1164 Simmonds, P.G., Derwent, R.G., Manning, A. J., McCulloch, A., and O'Doherty, S.: USA
1165 emissions estimates of CH₃CHF₂, CH₂FCF₃ and CH₂F₂ based on in situ observations at Mace
1166 Head. *Atmos. Environ.*, 104, 27-38, 2015.
1167
1168 SPARC Report on the Lifetimes of Stratospheric Ozone-Depleting Substances, Their
1169 Replacements and Related Species. SPARC Report No. 6. Edited by M.K.W. Ko, P.A.
1170 Newman, S. Reimann, and S. E. Strahan, WCRP-15/2013, December 2013.

1171
1172 Stohl, A., Forster, C., Frank, A., Seibert, P., and Wotawa, G.: Technical note: The Lagrangian
1173 particle dispersion model FLEXPART version 6.2, *Atmos. Chem. Phys.*, 5, 2461-2474, doi:
1174 10.5194/acp-5-2461, 2005.

1175
1176 Stohl, A., Seibert, P., Arduini, J., Eckhardt, S., Fraser, P., Grealley, B., Lunder, C., Miaone,
1177 M., Mühle, J., O'Doherty, S., Prinn, R., Reimann, S., Saito, T., Schmidbauer, N., Simmonds,
1178 P., Vollmer, M., Weiss, R., and Yokouchi, Y.: An analytical inversion method for
1179 determining regional and global emissions of greenhouse gases: sensitivity studies and
1180 application to halocarbons, *Atmos. Chem. Phys.*, 9, 1597-1620, 2009.

1181
1182 Stohl, A., Kim, J., Li, S., O'Doherty, S., Mühle, J., Salameh, P.K., Saito, T., Vollmer, M.K.,
1183 Wan, D., Weiss, R.F., Yao, B., Yokouchi, Y., and Zhou, L.X.: Hydrochlorofluorocarbon and
1184 hydrofluorocarbon emissions in East Asia determined by inverse modelling. *Atmos. Chem.*
1185 *Phys.*, 10, 3545-3560, 2010.

1186
1187 Sturrock, G. A., Porter, L.W., Fraser, P.J., Derek, N., and Krummel, P.B.: HCFCs, HFCs,
1188 halons, minor CFCs and halomethanes- The AGAGE in situ GC-MS program, 1997-1998,
1189 and related measurements on flask air samples collected at Cape Grim, in *Baseline Program,*
1190 *Australia 1997-1998*, edited by N.W. Tindale, N. Derek and R.J. Francey, pp.97-107, Bur. Of
1191 Meteorol, Melbourne, 2001.

1192
1193 Vollmer, M. K., Miller, B. R., Rigby, M., Reimann, S., Mühle, J., Krummel, P. B.,
1194 O'Doherty, S., Jim, J., Rhee, T. S., Weiss, R. F., Fraser, P. J., Simmonds, P. G., Salameh, P.
1195 K., Harth, C. M., Wang, R. H. J., Steele, L. P., Young, D., Lunder, C. R., Hermansen, O., Ivy,
1196 D., Arnold, T., Schmidbauer, N., Kim, K.-R., Grealley, B. G., Hill, M., Leist, M., Wenger, A.,
1197 and Prinn, R. G.: Atmospheric histories and global emissions of the anthropogenic
1198 hydrofluorocarbons HFC-365mfc, HFC-245fa, HFC-227ea, and HFC-236fa, *J. Geophys.*
1199 *Res.*, 116, D08304, doi:10.1029/2010jd015309, 2011.

1200
1201 Weiss, R. F., and Prinn, R.G.: Quantifying greenhouse-gas emissions from atmospheric
1202 measurements: a critical reality check for climate legislation, *Phil. Trans. R. Soc. A.*, 369,
1203 1925-1942, doi:10.1098/rsta.2011.0006, 2011.

1204
1205 Yao, B., Vollmer, M.K., Zhou, L.X., Henne, S., Reimann, S., Li, P.C., Wenger, A and M.
1206 Hill, M.: In-situ measurements of atmospheric hydrofluorocarbons (HFCs) and
1207 perfluorocarbons (PFCs) at the Shangdianzi regional background station, China, *Atmos.*
1208 *Chem. Phys.*, 12, 10181-10193, doi:10.5194/acp-12-10181, 2012.

1209
1210 Yokouchi, Y., Inagaki T., Yazawa, K., Tamaru, T., Enomoto, T and Izumi, K.: Estimates of
1211 ratios of anthropogenic halocarbon emissions from Japan based on aircraft monitoring over
1212 Sagami Bay, Japan. *J. Geophys. Res.*, 110, D06301, doi:10.1029/2004JD005320, 2005.

1213
1214 Yokouchi, Y., Taguchi, S., Saito, T., Tohjima, Y., Tanimoto, H and Mukai, H.: High
1215 frequency measurements of HFCs at a remote site in East Asia and their implications for
1216 Chinese emissions. *Geophys. Res. Lett.*, 33, L21814, doi:10.1029/2006GL026403, 2006.

1217

1218 Zhan T., Potts, W., Collins, J. F., Austin, J.: Inventory and mitigation opportunities for HFC-
 1219 134a emissions from nonprofessional automotive service, Atmos. Environ., 99, 17-23, 2014.

1220
 1221
 1222
 1223
 1224

1225 Table 1. Overview of the 11 Measurement Stations used in this Study, their Coordinates and
 1226 Periods for which Data are available.

Station	Latitude	Longitude	ADS Data*	Medusa Data**
Ny-Ålesund, Norway ¹	78.9° N	11.9° E	2001-2010	September 2010-present
Mace Head, Ireland ¹	53.3° N	9.9° W	1994-2004	June 2003-present
Jungfraujoch, Switzerland ¹	46.5° N	8.0° E	2000-2008	May 2008-present
Monte Cimone, Italy ²	44.2° N	10.7° E		June 2001-present ²
Trinidad Head, California ¹	41.0° N	124.1° W		March 2005 -present
Shangdianzi, China ^{1,3}	40.4° N	117.7° E		May 2010-August 2012
Gosan, Jeju Island, Korea ¹	33.2° N	126.2° E		November 2007-present
Hateruma, Japan ²	21.1° N	123.8° E		May 2004-present ²
Ragged Point, Barbados ¹	13.2° N	59.4° W		May 2005-present
Cape Matatula, Samoa ¹	14.2° S	170.6° W		May 2006-present
Cape Grim, Tasmania ¹	40.7° S	144.7° E	1998- 2004	Jan 2004-present

1227
 1228
 1229
 1230
 1231
 1232
 1233
 1234
 1235
 1236
 1237
 1238
 1239
 1240
 1241
 1242
 1243
 1244
 1245
 1246
 1247
 1248
 1249
 1250
 1251

¹ AGAGE stations

² Affiliated stations use a different pre-concentration system (non-Medusa) than the AGAGE stations, but comparable GC-MS analytical instruments (see Yokouchi et al., 2006, Maione et al., 2014).

³ Shangdianzi was only operational for a short period and is not included in the modelling studies.

* Period of HFC-152a data record using ADS-GC-MS.

** Period of HFC-152a data record using Medusa-GC-MS.

1252 Table 2. Estimates of global emissions of HFC-152a (Gg/yr \pm 1 σ) based on AGAGE in situ
 1253 measurements using the AGAGE 2-D 12-box model. Emission inventories as reported in
 1254 UNFCCC National Inventory Reports (2014 submission), EDGAR (v4.2) database and
 1255 recalculated from the UNFCCC data as described in the text.
 1256

Year	AGAGE (Gg/yr)	UNFCCC as reported (Gg/yr)	EDGAR (4.2) (Gg/yr)	UNFCCC including "unspecified" contribution (Gg/yr)
1994	7.3 \pm 5.6			
1995	7.9 \pm 7.4	1.0	7.3	8.8
1996	9.1 \pm 8.4	1.1	8.9	13.3
1997	11.3 \pm 8.6	1.3	10.3	15.4
1998	12.5 \pm 10.9	1.2	11.7	13.3
1999	14.4 \pm 11.2	1.4	13.2	14.0
2000	16.6 \pm 12.2	2.2	15.2	13.0
2001	18.4 \pm 13.4	3.5	15.9	15.4
2002	22.5 \pm 14.7	4.5	18.6	17.6
2003	26.3 \pm 15.3	4.7	20.6	17.7
2004	29.2 \pm 15.6	4.8	21.7	18.1
2005	35.8 \pm 14.7	4.3	23.0	16.5
2006	43.3 \pm 14.9	4.4	24.9	16.7
2007	48.1 \pm 17.6	4.4	26.4	16.8
2008	48.9 \pm 16.7	4.3	28.0	16.4
2009	48.0 \pm 16.4	4.6		17.6
2010	53.4 \pm 17.5	4.9		18.6
2011	54.4 \pm 17.1	5.0		19.3
2012	53.2 \pm 18.5	5.2		20.5
2013	52.5 \pm 17.8			
2014	52.5 \pm 20.1			

1257
 1258
 1259 Table 3. Annex 1 and non-Annex 1 global and regional emissions in Gg/yr averaged over two
 1260 3-year periods. Values in the final column are from the 12-box model, all other values are
 1261 from the combined Eulerian and Lagrangian model of Lunt et al. (2015). The global
 1262 estimates from the 12-box model are not in exact agreement with the combined Annex I and
 1263 non-Annex I emissions reported in Lunt et al. 2015. However, this is not unexpected, given
 1264 the vastly different transport and inversion models used to estimate these terms. We note that
 1265 the uncertainty range of the combined Annex I and non-Annex I estimates does overlap with
 1266 the uncertainty range from the 12-box model, and a similar growth in emissions is seen across
 1267 the two averaging periods.
 1268

3-year Averages	Europe	North America	East Asia	East Asia	GLOBAL	GLOBAL	GLOBAL
	Annex 1	Annex 1	Annex 1	Non-Annex 1	Annex 1	Non-Annex 1	12-Box model
2007–2009	6.4 (5.2-7.5)	28.0 (22.5-33.4)	0.4 (0.2-1.2)	5.8 (4.5-7.5)	35.2 (27.7-42.6)	6.6 (4.3-9.2)	48.5 (37.0-60.6)
2010–2012	5.2 (4.1-6.4)	31.6 (24.5-38.6)	1.0 (0.5-1.6)	6.0 (4.3-8.2)	40.2 (31.3-49.3)	6.6 (3.9-9.8)	53.9 (43.0-67.3)

1269

1270 Table 4. Australian HFC-152a emissions (Mg/yr, 3-year running averages) calculated from
 1271 Cape Grim *in situ* observations via ISC (ADS and Medusa data, uncertainty: ± 1 s.d.) and
 1272 inverse modelling using InTEM (Medusa data, range: 25th-75th percentiles); ISC, NAME
 1273 averages weighted by uncertainties, ISC InTEM average for 2004 is based only on InTEM
 1274 data.

1275

1276

YEAR	ISC	InTEM	ISC and InTEM average	ISC/InTEM ratio
1999	24 \pm 7			
2000	25 \pm 8			
2001	27 \pm 9			
2002	28 \pm 10	32 (31-34)	31 \pm 2	
2003	28 \pm 10	32 (29-33)	31 \pm 4	0.88
2004	29 \pm 10	31 (29-33)	31 \pm 2	0.94
2005	32 \pm 10	31(30-33)	31 \pm 4	1.03
2006	38 \pm 10	35 (32-38)	35 \pm 6	1.09
2007	51 \pm 15	41 (37-43)	42 \pm 6	1.24
2008	49 \pm 15	43 (41-47)	44 \pm 5	1.14
2009	52 \pm 15	68 (64-72)	65 \pm 8	0.76
2010	59 \pm 20	69 (64-74)	67 \pm 10	0.86
2011	56 \pm 15	72 (68-76)	69 \pm 7	0.78
2012	77 \pm 25			
2013	69 \pm 24			

1289

1290

1291

1292

1293

1294

1295

1296

1297

1298